Norwegian University
of Life Sciences

Master's Thesis 2023 60 ECTS
Faculty of Bioscience

Exploring LRRC8A's Role In Adipogenesis Across Various Fat Depots

Marwa Ali Omar
Master in Chemistry and Biotechnology

Master's Thesis 2023

Exploring *LRRC8A*'s Role In Adipogenesis Across Various Fat Depots

Marwa Ali Omar

Preface

My thesis focuses on exploring the processes of adipogenesis and the role of LRRC8A in order to gain an understanding of obesity and metabolic disorders. I was motivated by my curiosity, about the underlying mechanisms behind these health issues. Although starting my master in 2022 posed challenges due to COVID 19 it turned out to be an experience. Throughout my research on obesity I ensured that our findings were presented in a way that would be accessible to both students and researchers. The laboratory work was conducted at the EpiGen laboratory at Akershus University Hospital.

I would like to express my gratitude do Professors Yvonne Böttcher and Simen Rød Sandve for their guidance as my supervisors. I am also thankful for the mentorship, support and constructive feedback provided by postdoc Torunn Rønningen, which have greatly contributed to my progress. Additionally I appreciate the contributions made by Mai Britt Dahl, our groups engineer. Lastly I must acknowledge the support and motivation from my partner as well as the constant encouragement from my family.

Marwa Ali Omar

Sammendrag – Norsk

Denne masteroppgaven handler om å forstå kompleksiteten til adipogenese, med søkelys på *LRRC8A* sin rolle i adipocyttceller. I sammenheng med den økende forekomsten av fedme og relaterte metabolske lidelser, hadde denne studies som mål å forbedre vår forståelse og kunnskap om adipocyttceller, som er avgjørende for å håndtere disse globale helseutfordringene. Oppgaven satte søkelys på hvordan LRRC8A fungerer i både SAT og VAT fettceller, som begge har forskjellige innvirkninger på menneskets helse. Hovedmålet var å undersøke påvirkningen og effekten av *LRRC8A* på biologien og metabolismen til adipocytter. Dette innebar å studere *LRRC8A* sin rolle i prosessen med adipogenese ved å bruke pre-adipocyttceller fra SAT og VAT celler. I tillegg til dette hadde oppgaven som mål å avdekke de underliggende mekanismene som LRRC8A bidrar til aspekter ved adipocyttceller. For å oppnå disse målene, ble teknikker som siRNA mediert knockdown. Sanntid PCR, Western Blot-analyse og immunfluorescence-mikroskopi brukt. Metodene ble brukt for å analysere hvordan er det å undertrykke *LRRC8A* påvirker differensieringen og funksjonelle egenskaper til adipocytter. Resultatene viste at reduksjon av uttrykket av *LRRC8A* ved bruk av siRNA-mediert knockdown hadde en innvirkning på både SAT og VAT celler. Det påvirket markørene for utvikling av fettceller. Foreslått at LRRC8A spiller en rolle i prosessene til fettceller. Dessuten fremhever de distinkte responsene fra SAT og VAT celler på undertrykte LRRC8A hvordan dette genet har funksjoner i fettcelleutvikling som avhenger av typen vev. Disse funnene har et bredt spekter av mulige implikasjoner. Ved å forstå rollen til LRRC8A i å differensiere adipocytter, bidrar dette til ny kunnskap og til vår forståelse av fedme og metabolske fortsettelser. Resultatene indikerer at LRRC8A er involvert i adipocytter-differensiering og sannsynligvis fungerer sammen med andre differensierings markører, som er påvirket av LRRC8A knockdown. Derfor kan oppgaven gi nyttige data som er viktige for en bedre forståelse av de mekanistiske kretsene som ligger til grunn for fedme og fettvevs spesifikke effekter.

Summary - English

This master thesis embarked on a journey to understand the complexities of adipogenesis specifically focusing on *LRRC8A*'s role in adipogenesis. In the context of the increasing prevalence of obesity and related metabolic disorders this study aimed to enhance our knowledge on adipocyte biology, which is crucial in addressing these health challenges. The investigation primarily focused on how *LRRC8A* functions in SAT and VAT fat cells, both of which have distinct impacts on human health. The main objective was to examine the influence and effects of LRRC8A on the biology and metabolism of adipocytes. This involved studying its role in the process of adipogenesis using pre-adipocyte cells derived from SAT and VAT fat tissues. Additionally, the study aimed to uncover the underlying mechanisms by which LRRC8A contributes to aspects of adipocyte biology. To achieve these goals techniques such as siRNA mediated knockdown, real-time quantitative PCR, Western Blot analysis and immunofluorescence microscopy was employed. These methods allowed for an analysis of how suppressing *LRRC8A* affects the differentiation and functional characteristics of adipocytes.

The results showed that reducing the expression of LRRC8A using siRNA mediated knockdown had an impact on both SAT and VAT cells. It affected the markers of fat cell development. Suggested that LRRC8A plays a role in the processes of fat cells. Moreover the distinct responses of SAT and VAT cells to suppressing *LRRC8A* highlight how this gene has functions in fat cell development that depend on the type of tissue. These findings have a wide range of potential implications. By understanding the role of *LRRC8A* in differentiating adipocytes this research adds novel knowledge to our understanding of obesity and metabolic disorders. The results indicate that *LRRC8A* is implicated in adipocyte differentiation and likely works in concert with other early differentiation markers, that are affected by LRRC8A knockdown. Therefore, the study might provide useful data that are important for a better understanding of the mechanistic circuits underlying obesity and adipose tissue depot specific effects.

Table of contents

Abbreviations

ASCs	Adipose-derived Stem Cells
bFGF	Basic Fibroblast Growth Factor
BMI	Body Mass Index
DMEM/F12	Dulbecco's Modified Eagle Medium/ Nutrient mixture F12
DMSO	Dimethyl Sulfoxide
FBS	Phosphate-Buffered Saline
LRRC8A	Leucine Rich Repeat Containing 8
MQ	Milli-Q water - Deionized and distilled
MSCs	Mesenchymal Stem Cells
MWM	Molecular Weight Marker
OVAT	Omental Visceral Adipose Tissue
PBS	Fetal Bovine Serum
PenStrep	Penicillin/Streptomycin
PFA	Paraformaldehyde
PPARγ	Peroxisome Proliferator-Activated Receptor Gamma
PVDF	Polyvinylidene Fluoride
RNAi	RNA Interference
SAT	Subcutaneous Adipose Tissue
SDS	Sodium Dodecyl Sulfate
SDS-PAGE	Sodium Dodecyl Sulfate Polyacrylamide Gel Electrophoresis
siRNA	Short Interfering RNA
TBS	Tris-Buffered Saline
TBS-tween	Tris-Buffered Saline-Polysorbate 20
VAT	Visceral Adipose Tissue
VRACs	Volume-Regulated Anion Channels

Introduction and literature overview

Obesity has become a global health crisis that threatens lives worldwide (World Health Organization: WHO, 2021). Obesity has been linked with diabetes, heart diseases and certain cancers such as prostate cancer (Garg et al., 2013; Saha et al., 2023). It contributes also to an abnormal accumulation of fat cells within fat tissue (Figure 1) (Müller et al., 2022).

Obese fat tissue typically comprises two distinct regions, visceral adipose tissue (VAT) and subcutaneous adipose tissue (SAT) (Britton et al., 2011). SAT and VAT are the most important depots, alongside other depots like epicardial fat (Britton et al., 2011). Of the two regions, VAT shows more significant associations with metabolic disorders and diseases compared to its subcutaneous counterpart (Fox et al., 2007). A process known as adipogenesis drives this formation process; mesenchymal stem cells provide foundational material (Cristancho & Lazar, 2011).

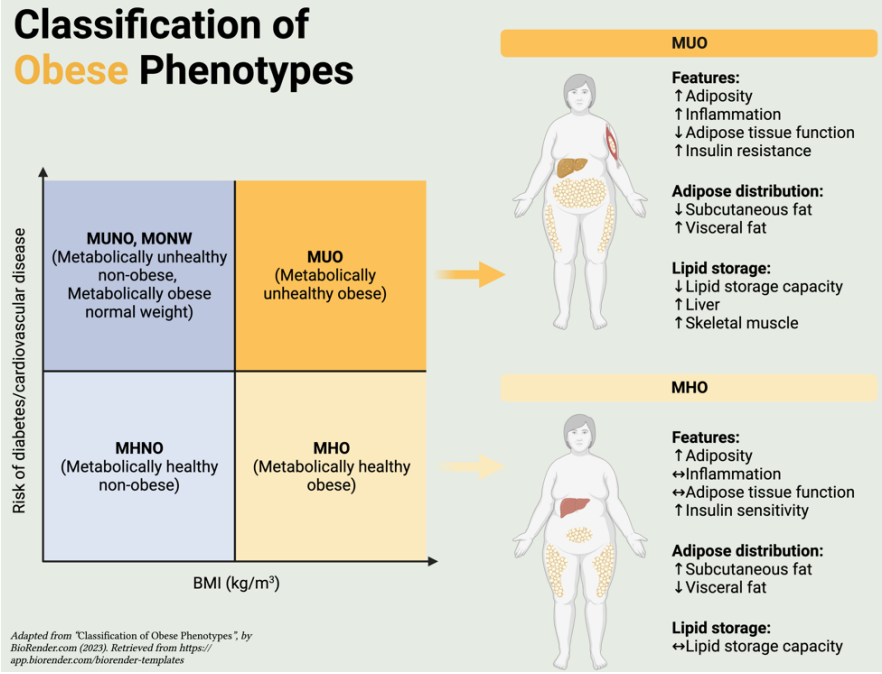

Figure 1 BMI-based Obesity and Metabolic Profiles – Adapted from "Classification of Obese Phenotypes", by BioRender.com (2023). Retrieved from https://app.biorender.com/biorender-templates.

Norway´s obesity problem continues to worsen, impacting both individual lives and healthcare system finances in adverse ways. (Midthjell et al., 2013) That is why encountering and managing this pandemic aren't optional; they are essential to overall well-being – financially as well as medically (Midthjell et al., 2013; Swinburn et al., 2011).

Body Mass Index (BMI) is often used as a way to gauge someone's weight status (F. F. Davidson et al., 2019); however, this measurement only looks at muscle and fat accumulation – not what kind of fat stores exist such as visceral/subcutaneous adipose tissue which was revealed in 2019 research conducted by Davidson et al. and World health Organization (Figure 2) (F. F. Davidson et al., 2019; (World Health Organization: WHO, 2021).

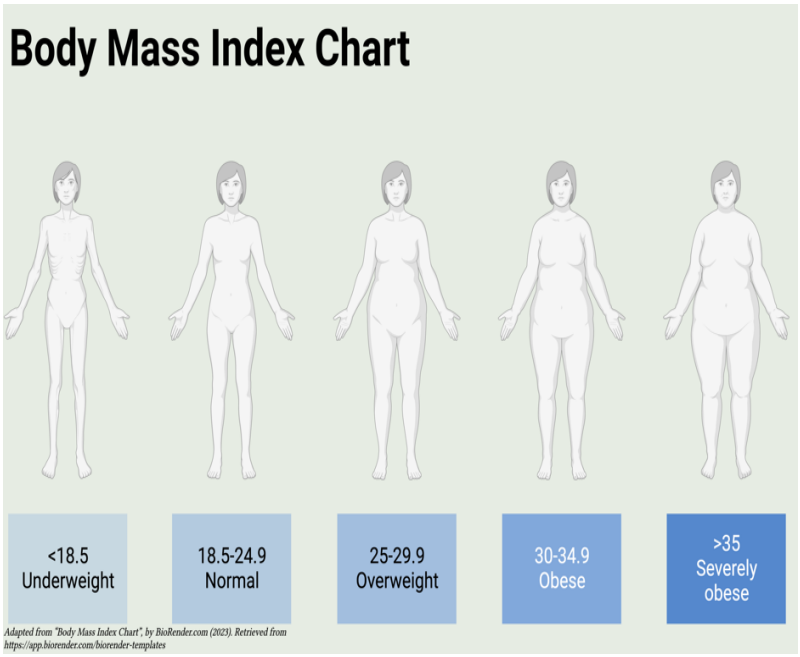

Figure 2 BMI Visual Reference Chart - Adapted from "Body Mass Index Chart", by BioRender.com (2023). Retrieved from https://app.biorender.com/biorender-templates.

Adipose tissue serves multiple roles in maintaining optimal body functions beyond acting as an energy store, including essential regulatory functions which should not be neglected or underestimated (Trayhurn, 2005). SAT and VAT are two primary fat depots found in humans with distinct metabolic properties and disease associations (Ibrahim, 2010). SAT lie beneath the skin layer; acting as a primary energy reservoir while protecting against metabolic disorders; while VAT accumulate within the abdominal region and has a correlation with increased risks for metabolic complications (Figure 3) (Ibrahim, 2010).

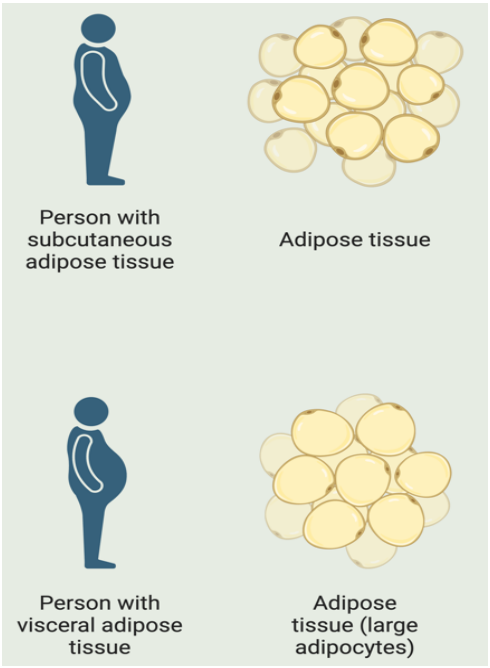

Figure 3 Subcutaneous vs. Visceral Fat - Adapted from "Icon Pack - Obesity (Human)", by BioRender.com (2023). Retrieved from https://app.biorender.com/biorender-templates.

Adipose depots are complex structures composed of many cell types that come together to form the fat tissue (Lee et al., 2013). Not only do mature adipocytes reside here; there are also mesenchymal stem

cells (MSCs), pre-adipocytes, macrophages, and lymphocytes present that all help shape its unique biomechanics (Lee et al., 2013).

Central to this system is adipose tissue, marked by Adipogenesis – the formation of fat cells or adipocytes (Cawthorn et al., 2012). Adipogenesis involves various factors which balance external signals with internal cell cues to stimulate differentiation of adipocytes (Cristancho and Lazar, 2011).

To effectively address and reduce the many complications brought on by obesity, we need a firm grasp on adipose tissue biology. This field has seen its own constant evolution over the last century or more; evidenced in its conversion of MSCs into the adipocyte lineage through MSC differentiation (Cawthorn et al., 2012).

Professor Yvonne Böttcher and her team at Akershus University Hospital (Ahus) are conducting intensive research into adipogenesis to gain greater insights into obesity and create innovative treatment approaches. Through comparative molecular characteristics analysis of VAT vs SAT, their researchers hope to shed new light into why VAT may be more associated with metabolic diseases than SAT, providing new understanding into this growing field (Fox et al., 2007). By understanding their differences more thoroughly this research area could guide better prevention or treatment approaches that could prevent and treat metabolic illnesses – which increasingly become prevalent worldwide, creating more effective strategies. Thus, it holds great potential impact.

My master thesis explores the role of LRRC8A in the formation of fat tissues from human preadipocytes. LRRC8A plays an essential part in volume-regulated anion channels (VRACs). VRACs play a vital role in controlling cell size regulation; without it functioning correctly it causes problems with size control leading to cell death (Qiu et al., 2014; Voss et al., 2014). We tested cells from two distinct fat tissues, SAT and VAT. We utilized siRNA to study how LRRC8A works by knocking down its expression levels using siRNA.

Introduction to Adipocyte Biology, Metabolism, and Adipogenesis

VAT (visceral adipose tissue located around our organs), and SAT (subcutaneous adipose tissue located under our skin), have enormous impact on human health (Britton et al., 2011). Excessive accumulation of VAT increases our risk for metabolic conditions like insulin resistance, diabetes, and cardiovascular diseases as it contains various metabolic and endocrine properties such as secreting harmful adipokines through its connection to liver (Figure 4) (Garg et al., 2013). Therefore studying VAT helps identify those at high risk and create tailored interventions (Tchernof & Després, 2013).

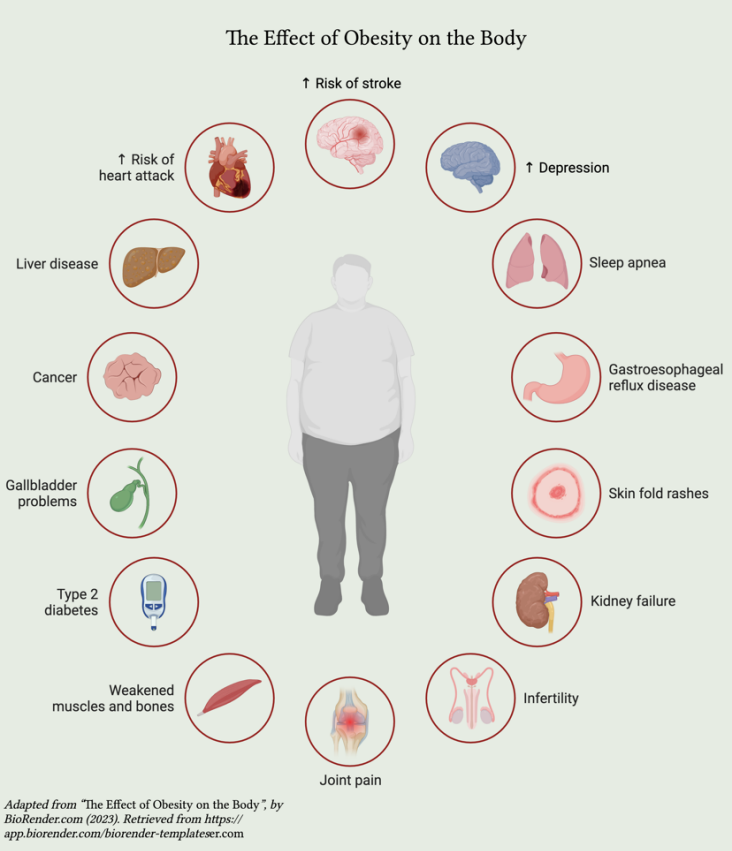

Figure 4 Health Complications of Obesity - Adapted from "The Effect of Obesity on the Body", by BioRender.com (2023). Retrieved from https://app.biorender.com/biorender-templateser.com.

Adipose tissue is made up of types of fat cells; white, brown, and beige (Kaisanlahti & Glumoff, 2019). Each playing a unique role in energy metabolism. White fat cells store energy while brown and beige fat cells are involved in generating heat (Figure 5) (Kaisanlahti & Glumoff, 2019).

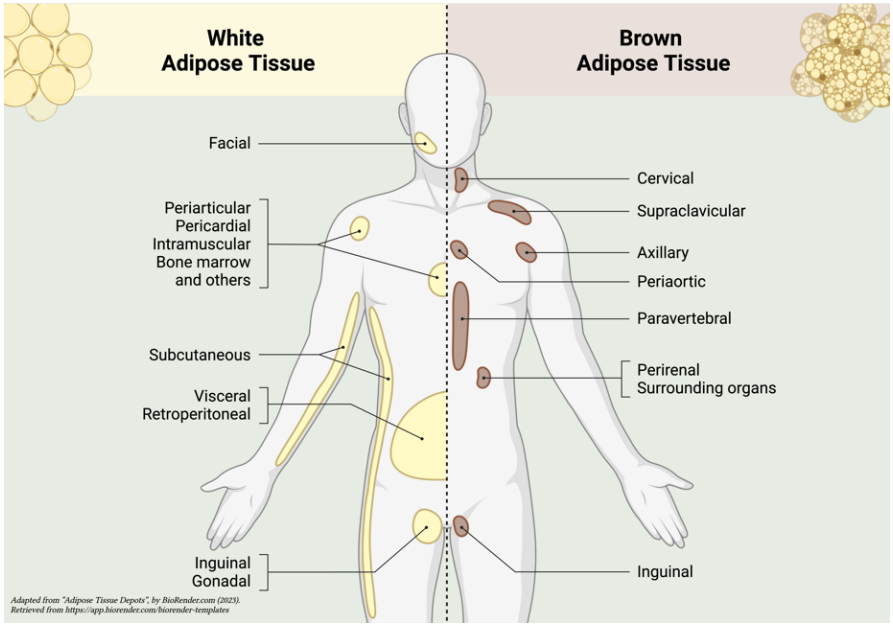

Figure 5 Body Fat Distribution: White vs. Brown - Adapted from "Adipose Tissue Depots", by BioRender.com (2023). Retrieved from https://app.biorender.com/biorender-templates.

Environmental factors also have a role in influencing processes like adipogenesis (Zhu *et al.*, 2021). Lifestyle choices, level of activity and exposure to chemicals can affect adipogenesis by interacting with predispositions that modulate health risks (Cristancho and Lazar, 2011). For example, diets high in saturated fats can speed up adipogenesis leading to the accumulation of tissue and increased risks for metabolic syndrome (Zhu *et al.*, 2021). On the other hand, a balanced diet have effects on these processes highlighting how adaptable our biological system are and how lifestyle changes can help manage metabolic disorders (Zhu *et al.*, 2021). The maintenance of energy balance relies on the process of adipogenesis which is influenced by signaling pathways and transcription factors that control gene transcription (Cristancho and Lazar, 2011).

In fat tissues, cells such as pre-adipocytes and MSCs, play crucial roles. Pre-adipocytes are responsible for producing adipocytes while MSCs influence responses and can differentiate into various cell types (Ghaben and Scherer, 2019). Adipocytes develop from MSCs under the influence of factors like bone morphogenetic protein (BMP) and Wnt signaling pathways process (Pant *et al.*, 2021). Various transcription factors and proteins like peroxisome proliferator-activated receptor gamma (PPARγ) and CCAAT/enhancer-binding proteins (C/EBPs) also

contribute to this process (Pant *et al.*, 2021). These pathways, including insulin/IGF, Wnt/β-catenin and TGF-β pathways can promote or hinder adipocyte development (Rosen & MacDougald, 2006).

Fat tissue adjusts to changing energy requirements by maintain a balance between energy storage and usage (Pant *et al.*, 2021). Environmental signals, cues, as well as transcription regulators, help regulate this balance (Pant *et al.*, 2021). A comprehensive understanding of adipogenesis is crucial for developing treatments for obesity and related conditions (Pant *et al.*, 2021).

The Impact of Obesity on Adipocyte Biology and Metabolism

Obesity triggers chronic inflammation within its fat tissues further worsening insulin resistance; this includes immune cell infiltrations, stress-responsive pathway activation and increased production of pro-inflammatory cytokines (Kusminski et al., 2016; Saltiel & Olefsky, 2017). Expanded fat tissue due to obesity can lead to hypoxia, or lack of oxygen, leading to inflammation and fibrosis – an excessive build-up of extracellular matrix components in fat tissues that leads to their dysfunction and ultimately leads to insulin resistance (Figure 6) (Trayhurn, 2013; Kusminski et al., 2016). Any disruption in the secretion of adipokines such as leptin, adiponectin and resistin which regulate energy metabolism, insulin sensitivity and inflammation can result in insulin resistance and later type 2 diabetes (Kusminski et al., 2016).

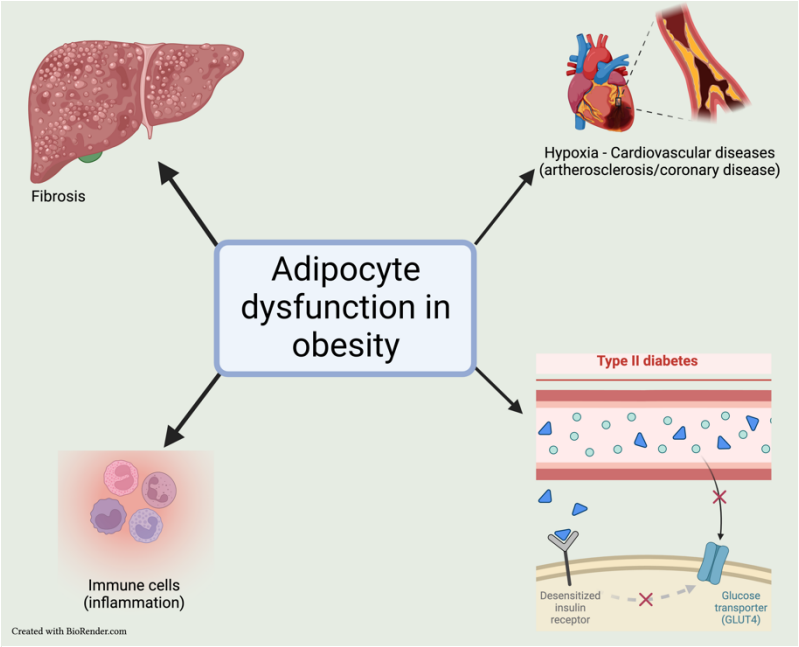

Figure 6 Consequences of Adipocyte Dysfunction - Created with BioRender.com.

Unfortunately, obesity can act as a catalyst for altering this delicate balance between these fat cells, by interfering with energy metabolism overall; consequently, even leading up to obesity-

related diabetes (Villarroya et al., 2017). To address this issue, scientists are exploring targeted interventions that focus on specific adipose tissue, aiming to rectify these concerns. For example, "browning" the tissue or modifying the differentiation process of fat cells is one approach being considered along with reducing inflammation levels along adipokine secretion enhancement carried out through signalling pathways found associated with dysfunction in adipose tissues (Kusminski et al., 2016; Scheja & Heeren, 2019).

In the current era of widespread obesity, where addressing the increasing prevalence of excess weight is crucial, treatment targeting dysfunctional fat tissue is essential. A comprehensive approach is required to address the metabolic disturbances caused by inactive adipose tissue during low-calorie periods in obese individuals (Scheja & Heeren, 2019).

Further research should aim at better comprehending the complex relationship between fat tissue dysfunction and obesity-related diabetes, including personalized therapeutic strategies designed for obesity-related diabetes patients. To advance personalized treatments for obesity related diabetes, it is essential to delve deeper into the factors influencing adipose tissue functionality – this would improve quality of life while decreasing healthcare burden associated with metabolic disorders. Potential research areas might include exploring root causes, genetic, lifestyle factors impact, roles played by other adipokines such as TGF or its receptor, progress, potency potential of therapeutic strategies used against metabolic disorders.

Tracing The Evolution of RNA Modifications from Pseudouridine To m6A

Epitranscriptomics is an emerging field that studies changes to RNA molecules that affect their functions and gene expression (Zhao et al., 2017). Studies of RNA modifications, particularly methylation, have been ongoing since their first discovery – pseudouridine in the 1950s (Cohn, 1960). But with next-generation sequencing technologies coming online in 2000s we were finally able for map these modifications across transcriptome-wide levels, hence creating the field of epi-transcriptomics (Mardis, 2008; Meyer & Jaffrey, 2017).

The 2011 discovery of demethylase fat mass- and obesity-associated protein (FTO) revolutionized our understanding of RNA methylation; showing it is not static but dynamically regulated (Jia et al., 2011).

The study of RNA modifications has uncovered over 170 types of posttranscriptional RNA modifications, but their rolls are still not fully understood (Boccaletto et al., 2021). One of the most investigated modifications is methylation, specifically methyl6A or m6A, which has significant effects on both RNA functionality within cells and cellular processes overall (Figure 7) (Dominissini et al., 2012; Meyer & Jaffrey, 2017). There is compelling evidence that links m6A with the development of adipocytes or fat cells.

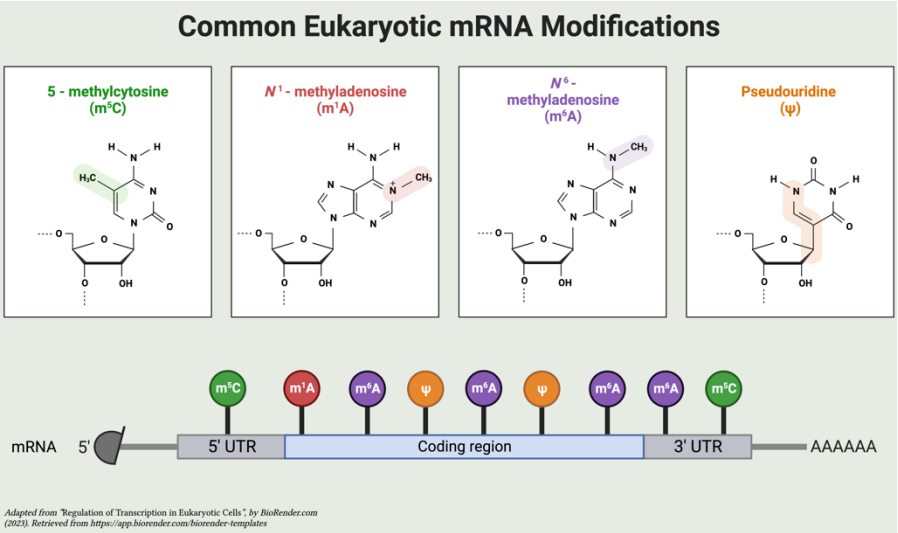

Figure 7 Types of mRNA Modifications in Eukaryotes - Adapted from "Regulation of Transcription in Eukaryotic Cells", by BioRender.com (2023). Retrieved from https://app.biorender.com/biorender-templates.

For instance, one widely studied change – known as m6A – is reversible and controlled by specific proteins such as writer, eraser and reader proteins (Yang *et al.*, 2018). These proteins play roles in controlling RNA metabolism and have significant implications for various physiological processes and disease (Yang *et al.*, 2018). Writer protein, such as WTAP, KIAA1429 and RBM15/RBM15B are part of the methyltransferase complex (Yang *et al.*, 2018). They are essential for regulating m6A levels on RNA transcripts (Yang *et al.*, 2018). For instance, WTAP plays a role in localizing the METTL3 METTL14 complex, which is important for pre mRNA processing (Yang *et al.*, 2018). Similarly, KIAA1429 and RBM15/RBM15B have been found to be involved in region m6A methylation guidance and directing the methylation of adenosine residues respectively (Yang *et al.*, 2018). Eraser proteins like FTO and ALKBH5 function as demethylases responsible for removing m6A modifications from RNA (Yang *et al.*, 2018). This makes the process dynamic and reversible. FTO specifically has been associated

with modifications derived from m6A in mRNA molecules, is involved in regulating gene expression by affecting interactions between RNA molecules and proteins (Yang *et al.*, 2018). ALKBH5, which is another demethylase enzyme has been discovered to have involvement in processes like spermatogenesis and cerebellar development (Yang *et al.*, 2018). It affects the export and metabolism of mRNA (Yang *et al.*, 2020). Reader proteins, specifically members of the YTH domain family, are responsible for identifying and interpreting m6A sites on transcripts (Yang *et al.*, 2018). Their role is crucial in determining the destiny of target mRNAs influencing mRNA degradation, translation efficiency and overall gene expression (Wang *et al.*, 2022). These discoveries emphasize the vital role that m6A modification plays in RNA biology. Gaining understanding about the functions of these writer, eraser and reader proteins is essential for unraveling the mechanisms behind RNA regulation and their implications across processes and diseases.

Future studies should investigate how regulatory enzymes direct RNA modifications (Boccaletto et al., 2021). Investigating these areas could provide greater understanding into RNA modifications and could reveal therapeutic targets for metabolic diseases (Boccaletto et al., 2021).

Functional Analysis of Differentially Methylated Transcripts in Pre-Adipocyte cells

The choice to focus on *LRRC8A* as a target gene derives from the research priorities within Yvonne Böttcher's team at Akershus University Hospital (Ahus). The team concentrates on elucidating the mechanisms underlying the heightened association between the expansion of visceral adipose tissue and metabolic disease, achieved though the comparative study of molecular characteristics in subcutaneous versus visceral adipose tissues. A forthcoming publication from the group (Rønningen et al., in preparation) explores discrepancies in RNA methylation – specifically, N6-methyladenosine (m6A) – in subcutaneous and visceral adipocytes. The study identified *LRRC8A* as a gene showing divergent methylation between these two types of adipocytes, notably with an elevation in methylation within the 3'untranslated region (UTR) in visceral adipocytes when contrasted with their subcutaneous counterparts. Consequently, our current research aims to investigate the functional role and potential depot-specificity of *LRRC8A* during adipogenesis. To this end, we are employing pre-adipocytes from

subcutaneous and visceral adipose tissue depots to observe any depot-specific differences that might exist.

To examine adipocytes, several transcription factors play a vital role in turning pre-adipocytes into mature fat cells; one such transcription factor, known as Peroxisome Proliferator-Activated Receptor Gamma (PPARγ), play an integral part (De Sá et al., 2017). Another transcription factors like CCAAT/Enhancer Binding Proteins (C/EBPs) play important roles in developing obesity and type 2 diabetes (De Sá et al., 2017). Co-regulators, proteins that work with transcription factors, are critical in the differentiation process for fat cell development and any imbalance can lead to metabolic diseases (De Sá et al., 2017).

The Leucine Rich Repeat Containing 8 Family (LRRC8) and its role in adipocyte biology and metabolism.

Understanding VRAC heteromers has deepened our knowledge regarding their structure, function, and regulation. These proteins appear to participate in cell proliferation, migration, apoptosis, as well as disease like cancer of ischemia (Stauber, 2015). Voss et al. (2014) has provided us with valuable insight into LRRC8 heteromers as VRAC components, their biophysical characteristics, molecular composition, and physiological roles. VRAC plays an essential role in channel activity while subunits such as LRRC8B-D can later channel properties (Qiu et al., 2014; Jentsch & Pusch, 2018). Their involvement with cell proliferation, migration apoptosis diseases underline our need to comprehend both their function and regulation (Pedersen et al., 2015).

LRRC8A, more commonly called SWELL1 (from swelling 1), has been shown to have an important role in adipocytes. LRRC8A forms and activates fat cells' VRACs. Furthermore, LRRC8A enable VRAC-mediated adipocyte processes such as adipogenesis, insulin sensitivity and lipolysis (Figure 8) (Jentsch et al., 2016; Strange et al., 2019).

Without LRRC8A, functioning of VRACs would cease completely; working together with its family members (LRRC8B-E), LRRC8A can fine-tune channel properties for improved understanding of VRAC function and regulation (Stauber, 2015).

An understanding of LRRC8A function provides key insight into health conditions like obesity or type 2 diabetes. LRRC8A play an essential role in activating various isoforms of LRRC8; particularly VRACs consisting of various isoforms (Strange et al., 2019). Without LRRC8A, these isoforms would neither form functional VRACs nor engage in their regulatory activity (Strange et al., 2019. Further research should be completed to gain greater insight into molecular interactions between LRRC8A and other isoforms of LRRC8. Furthermore, LRRC8A also plays an essential role in energy storage and metabolic regulation by adipocytes – primary energy stores and regulators (Jentsch et al., 2016; Strange et al., 2019).

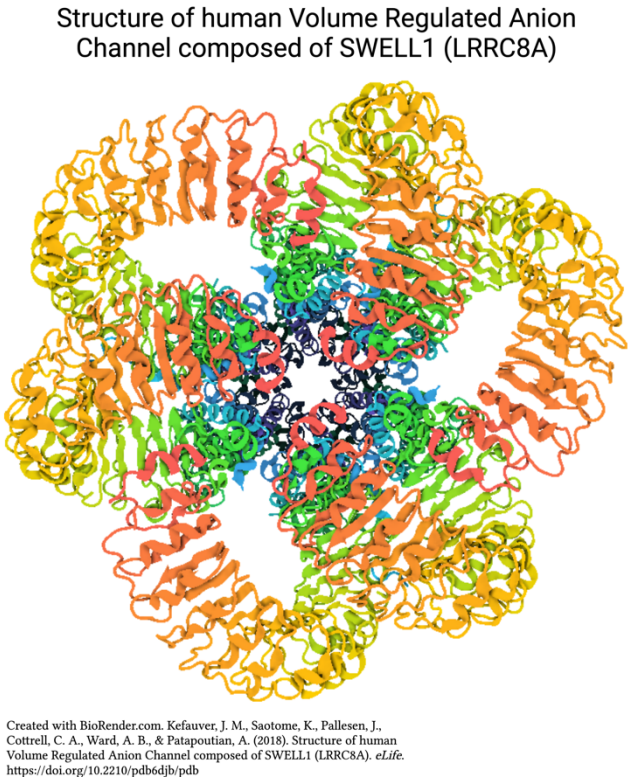

Figure 8 SWELL1 (LRRC8A) Channel Structure – Figure Created with BioRender.com. Structure adapted from Kefauver, J. M., Saotome, K., Pallesen, J., Cottrell, C. A., Ward, A. B., & Patapoutian, A. (2018). Structure of human Volume Regulated Anion Channel composed of SWELL1 (LRRC8A). eLife. https://doi.org/10.2210/pdb6djb/pdb.

Studies have demonstrated how VRACs containing LRRC8A contribute to release of adiponectin which improves insulin sensitivity, fat oxidation and Taurine transport (an amino acid involved with glucose homeostasis), making LRRC8A and VRACs potential therapeutic

targets against metabolic diseases (Jentsch et al., 2016; Strange et al., 2019). Insulin sensitivity is crucial in maintaining stable glucose levels and avoiding type 2 diabetes; Rocha et al.'s research on this relationship clarified this point. The researchers found that LRRC8A is essential in helping fat cells (adipocytes) absorb glucose when stimulated with insulin; should its function become impaired, it significantly reduces glucose uptake into fat cells known as adipocytes (Figure 9) (Jentsch et al., 2016; Strange et al., 2019).

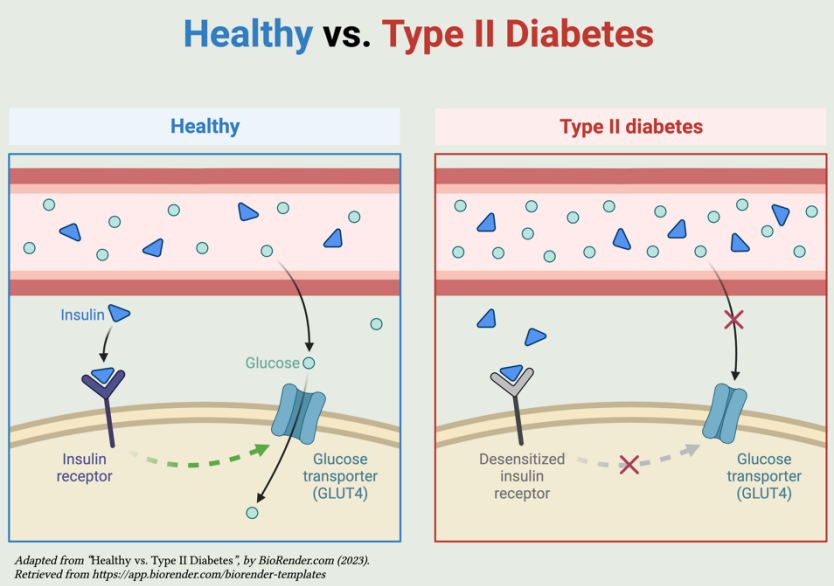

Figure 9 Healthy vs. Diabetic Glucose Transport - Adapted from "Healthy vs. Type II Diabetes", by BioRender.com (2023). Retrieved from https://app.biorender.com/biorender-templates.

Rocha et al.'s research indicate that LRRC8A plays an essential role in the effectiveness of insulin by helping fat cells respond to its stimulation. Any disruption may compromise signalling systems or decrease insulin sensitivity, resulting in worsen inflammation and diminishing treatment responsiveness (Rocha et al., 2021).

Zhang et al. 2015 investigated adipogenesis – forming of new fat cells - using 3T3-L1 cells and noticed increased *LRRC8A* expression during this stage. The researchers further noticed that suppressing *LRRC8A* with siRNA can prevent differentiation into new adipocytes suggesting its crucial role in lipogenesis and the process of adipogenesis.
VRAC channels with LRRC8D sequence have been tied with regulation of lipolysis while those containing this sequence increase insulin sensitivity, this makes LRRC8A an integral component in both biology and metabolism of adipocytes (Jentsch et al., 2016; Strange et al., 2019).

Research LRRC8 isoforms has proved instrumental to our efforts at combatting obesity and related metabolic disorders with personalized medicine. However, knowledge gaps still need to

be filled. Clarifying the molecular pathways and signals by which LRRC8 isoforms exert influence over adipocyte functions is of critical importance; their roles within metabolism must also be studied closely since isoforms such as LRRC8B, C, and E are so fundamental in understanding adipocyte development. An understanding of how tissue-specific expression of LRRC8 isoforms affect various forms of adipose tissue is still incomplete and calls for more research. Uncovering these areas is crucial in order to gain more insights into LRRC8 isoforms and VRAC channels and develop therapies for obesity as well as related metabolic conditions such as inflammation of adipose tissue as well as immune cell functions which might shed additional light into relationships among adipocyte function, inflammation, immune cell functions and health status (Jentsch et al., 2016; Strange et al., 2019).

As obesity rated and metabolic disorders present increasingly serious health challenges to society, including type 2 diabetes, cardiovascular diseases, and certain cancers (Figure 10) (Garg et al., 2013; Saha et al., 2023). It is imperative that we gain further insights into molecular mechanisms regulating adipocyte function to develop novel solutions against its health consequences. Studies of LRRC8 isoforms and VRAC channels play a central role in the function and metabolism of adipocytes. Understanding their impact may provide novel targets or treatments for related disorders. Further, LRRC8's many isoforms with differing VRAC channel properties are indicative of its complexity in adipocyte biology. By exploring tissue-specific expression patterns and functional roles for individual isoforms of LRRC8, we may gain greater insights into interactions among adipocyte function, inflammation, metabolic health and more. Furthermore, exploring how LRRC8 isoforms and VRAC channels contribute

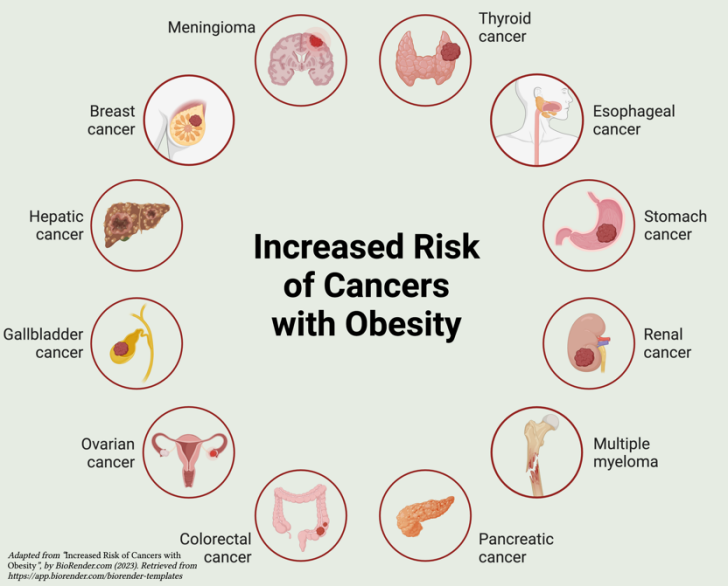

Figure 10 Obesity-Related Cancer Risks - Adapted from "Increased Risk of Cancers with Obesity", by BioRender.com (2023). Retrieved from https://app.biorender.com/biorender-templates.

to thermogenesis and browning of white adipose tissue for new regulatory strategies (Jentsch et al., 2016; Strange et al., 2019).

Investigating interactions between LRRC8 isoforms and other ion channels or transporters is key to unlocking insights into adipocyte biology and providing potential therapeutic targets. Research along these lines and identification of therapeutic targets could give researchers greater insights into how LRRC8 isoforms and VRAC channels influence adipocyte biology and metabolism, possibly opening doors to developing effective new treatments for obesity-related metabolic conditions (Jentsch et al., 2016; Strange et al., 2019).

Studies have demonstrated how impairment can alter cellular signalling, making regulation more complex. LRRC8A is crucial in this context, as its absence can hinder essential signals transduction mechanisms as well as transmission pathways, affecting both the transmission and processing of signals within cells (Jentsch et al., 2016; Strange et al., 2019).

Recent research has provided insights into the effect of LRRC8A on the adipocyte differentiation process. Lacking this molecule stops cell formation by disrupting mitochondrial biogenesis, intracellular calcium balance, and microRNA expression associated with adipogenesis. These discoveries show its significance within adipocytes, as its actions affect fat storage and glucose metabolism. Therefore, targeting this molecule could potentially provide new therapeutic strategies against obesity and its related metabolic

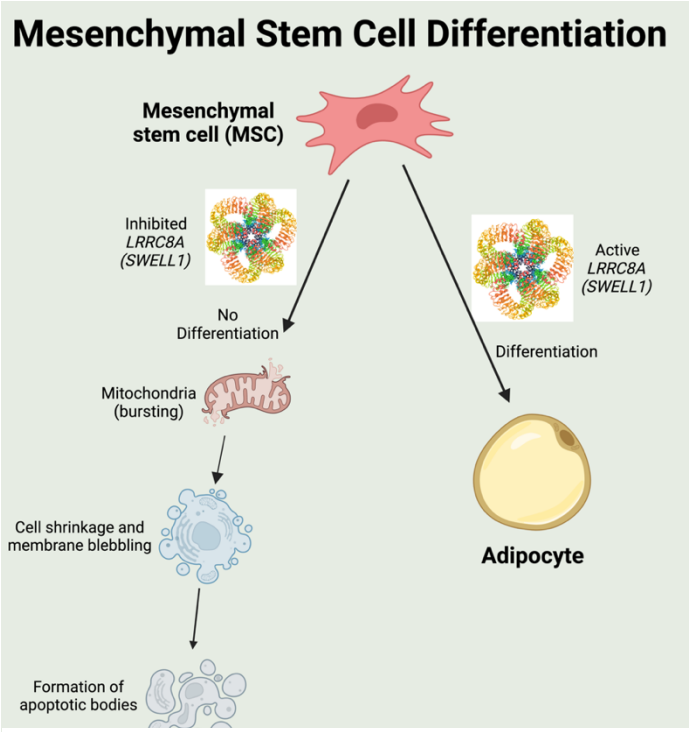

Figure 11 MSC Differentiation and LRRC8A Influence

conditions (Figure 11) (Jentsch et al., 2016; Strange et al., 2019).

Study of LRRC8A protein has provided insights into how adipocytes operate; yet despite our progress there remain gaps in our knowledge of this cell type. Examining how this protein acts within various types of fat cells such as brown, white and beige fat tissue is paramount; its impact can have far reaching ramifications on development and breakdown processes as well as contributing towards creating new mitochondria and maintain calcium levels in our bodies. Most studies focusing on LRRC8A expression in muscle tissues have relied upon laboratory experiments or mouse models lacking such expression (Chen *et al.*, 2022). But to truly enhance our knowledge we need to broaden research efforts by including living organisms who express LRRC8A regardless of any abnormalities present in their tissue structure. Finally, LRRC8A holds great promise as a target for treating obesity and related conditions. Before we can make this idea a reality, however, a comprehensive understanding its therapeutic potential must first be acquired – including considering safety measure, effectiveness of treatments methods as well as potential complications linked to manipulating its activity or delivery techniques.

Thesis aims and objectives of the study.

Our research investigated weather *LRRC8A* played an influential role in human adipogenesis through different tissue types, SAT and VAT.

The objectives of the study:

1. Investigate the role and impact of *LRRC8A* in the biology and metabolism of adipocytes. To do this, we will use siRNA knockdown techniques to study how it affects differentiation. Furthermore, we will optimize our siRNA techniques.
2. Examine how *LRRC8A* influences adipogenesis in cells derived from SAT and VAT.
3. Uncover the mechanisms through which *LRRC8A* is involved in adipocyte biology. This will help us understand its contribution to the differentiation and development of cells.

Materials and Methods.

Pre-adipocyte cells

Both pre-adipocytes from subcutaneous adipose tissue (SAT) and omental visceral adipose tissue (OVAT) were purchased commercially from Zen-Bio (NC, USA**).** We used pre-adipocytes with passage numbers between 5-9 for all experiments.

Cell culture work

Cell culture work required precise handling of reagents under sterile conditions, including media preparation and protocols for thawing frozen cell aliquots for seeding, cell growth, cell counting, and splitting (Figure 12).

The reagents used included DMEM/F12 (Dulbecco's Modified Eagle Medium/ Nutrient mixture F12) medium, phosphate-buffered saline (FBS), Penicillin/Streptomycin (PenStrep), basic Fibroblast Growth Factor (bFGF), cell culture flasks/plates, TrypLE express, and Fetal Bovine Serum (PBS) (Table 3).

The preparation of cell culture medium

The basal medium

The basal medium comprised DMEM/F12, 10% FBS, and 1% PenStrep. To prepare the basal medium, 56 ml of FBS and 5.6 ml of PenStrep were aseptically added to a full bottle (500 ml) of DMEM/F12. We then stored the medium at -20 °C until further use. For transfection experiments, we took aliquots of DMEM/F12 with 10% FBS before adding PenStrep and stored them at -20 °C.

The proliferation medium

The proliferation medium comprised DMEM/F12, 10% FBS, 1% PenStrep, and 1ng/ml bFGF. To prepare fresh proliferation medium, 50 µl of a 1 µg/ml bFGF solution was added to 50 ml of the basal medium in a 50 ml falcon tube.

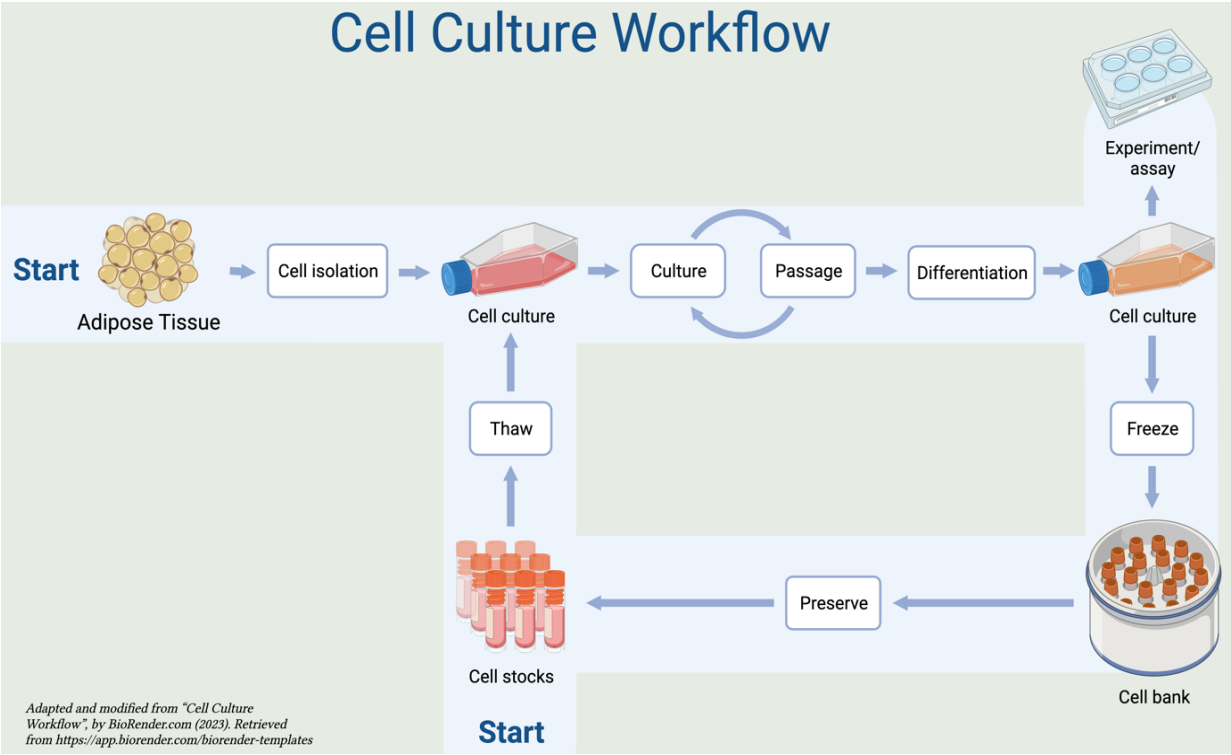

Figure 12 Stages of Adipose Tissue Cell Culture and Storage

Thawing of cells from storage (-150 °C)

We followed the detailed protocol, which involved pre-warming the cell culture medium to 37 °C, after which we transferred 9 ml of the basal medium to a 15 ml falcon tube to thaw cells from storage. After retrieving the cell vial from -150 °C storage, we thawed it at 37 °C. The fully thawed cell suspension was quickly and carefully added to the basal medium in the falcon tube to avoid the toxic effects of Dimethyl sulfoxide (DMSO) on cells. Centrifugation of cells was conducted at 300 g for 10 minutes at room temperature. We carefully discarded the supernatant with a pipette. Depending on the number of cells per vial, we resuspended the cell pellet in the correct volume of the basal medium. We used 175 cm^2 flasks for cell counts greater than 1 million and 75 cm^2 flasks for cell counts less than 1 million. We replaced the medium with a proliferation medium on the following day.

Cell passaging/splitting

Normally the cells were split twice a week. The protocol for cell passaging from 175cm^2 flasks is shown below and involves allowing the cells to reach a confluency of 70-80% before initiating

the process. We ensured that pre-adipocytes were seeded tightly, as they grow better when in contact with adjacent cells. We avoided confluence to prevent hindering proliferation and causing premature differentiation, which we did not desire.

We started by warming up PBS, TrypLE Express and the proliferation medium, to a temperature of 37 °C. Then we removed the existing medium using an aspirator system. For a flask with a size of 75 cm^2 we used 10 ml of PBS and for a flask with a size of 175 cm^2 we used 20 ml. after rinsing the cells with PBS we carefully aspired it. Added TrypLE Express allowing it to incubate until the cells detached. To neutralize TrypLE Express we used a mixture of proliferation medium in a ratio of 4:1. Then we divided the cells into flasks at a ratio of 1:5. Added the required medium and finally each flask was labeled with information including cell type, passage number and date.

We evenly distributed the cells in the flask by gently moving them back and forth in an 8-shaped motion. We cultured the cells in a humidified incubator at 37 °C with 5% CO2. We conducted daily inspections of the cells using a microscope. The culture media was replenished with a new proliferation medium every 3 to 4 days.

Cell counting

Cell counting was performed by removing 10 µl of the cell suspension into an Eppendorf tube and adding 10 µl of Trypan Blue, followed by thorough mixing. Subsequently, we transferred 10 µl of the suspension to one chamber of a counting slide and used both chambers to calculate the average of the two cell counts. We used the clear blue ring and bright interior that the viable cells exhibited to determine the viable cell count number for calculation. We disregarded background materials due to their potential to produce false positives.

Cell seeding

When seeding cells for experiments after cell counting, it was necessary to follow a detailed protocol (Figure 13). The process included steps such as labelling a new flask with essential information, which included the cell name, passage number, and date. Additionally, we had to add the appropriate volume of proliferation medium to reach the desired total volume,

considering both the current and desired cell counts in each flask. For instance, 2.5 ml of cells were added to 27.5 ml of proliferation medium to achieve the desired cell count.

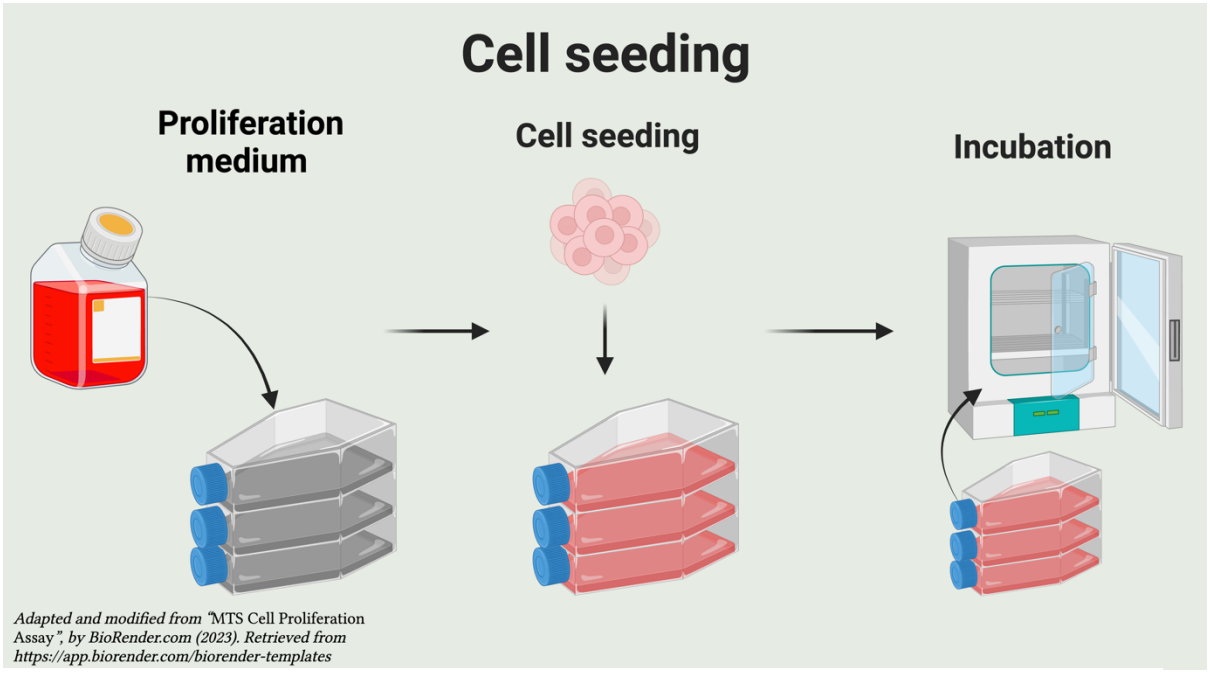

Figure 13 Cell Culture Process Overview

Freezing cells

We conducted the preservation of cells through freezing using the following procedure.

We trypsinized the cells using a previously established method, diluted the TrypLE Express with 4X basal medium, and then transferred it to a falcon tube. The mixture was centrifuged at 300g for 10 minutes to form a cell pellet. The cell pellet was then resuspended in 1ml of basal medium per vial to be frozen and mixed thoroughly. We then labelled each cryotube with the relevant information, including cell name, passage number, date, and cell number. 50 µl of DMSO was added to the cell suspension, resulting in a final concentration of 5%. The cells were immediately transferred to a CoolCell box for gentle freezing and stored at -80 °C. The next day, we transferred the cells to a storage temperature of -150 °C and updated the storage list in the group's shared drive.

ORO Staining - and Microscopy of Adipocytes

Oil Red O (ORO) is a reliable and cost-effective stain for quantitative and qualitative measurement of lipid droplet formation. However, we can only use it to analyse dead cells.

While it provides intense red colourations, its efficacy is limited for high throughput analysis (Majka *et al.*, 2014; Sikkeland, Jin and Saatcioglu, 2014).
We captured the microscope images using the ZEISS Axio Vert.A1, an inverted microscope designed for live cell investigations.

I. We followed a specific protocol for the 6-well plate for the fixation of cells with PFA on days 9 and 14 of the differentiated adipocyte experiment. We removed the cell culture medium and washed cells twice with 1 ml PBS per well. Cells were fixed by adding 2 ml of 4% PFA per well and incubated for 1 hour at room temperature while kept inside the LAF bench. We removed the PFA and washed cells twice with 1 ml PBS per well. If required, the cells were stored in 2 ml PBS per well at 4 °C before proceeding with staining. This step was performed for day 9 samples to enable simultaneous processing of day 9 and day 14 samples. Finally, we sealed the plates with parafilm.

II. Preparation of Oil Red Solution: (Could be carried out outside the LAF bench)
We prepared a 0.5% ORO stock by adding 0.25g of ORO to 50 ml of 96% EtOH. We could store the ORO stock for an extended period in the fridge. We prepared the ORO dilution for two 6-well plates by mixing 18 ml of ORO stock with 12 ml of MQ water. The solution was thoroughly vortexed and incubated at room temperature for 5-10 minutes. The solution was then filtered through Whatman paper filters and left on the bench until all the solution had passed the filter for around 30 minutes.

I. Staining of cells with Oil Red O: (Could be carried out outside the LAF bench)
We removed all PBS from the wells. The wells were washed once with 2 ml of freshly prepared 60% isopropanol diluted with MQ water. Removed all isopropanol and added 2 ml of filtered ORO to each well. We incubated the cells for 1 hour with gentle horizontal shaking. After incubation, we removed the ORO staining and washed the wells 2-3 times with 2 ml of 60% isopropanol until we observed apparent background staining. We removed the isopropanol and washed the wells once with 2 ml PBS. 2 ml PBS was added to each well at the end to prevent drying out. We took

pictures of all four wells using a light microscope at 10X, 20X and 40X magnification. Finally, we sealed the plates with parafilm and stored them at 4 °C.

Western blot analysis

Western blotting is a protein detection technique that can determine distinct proteins' presence, size, and semi-quantitative expression levels. We must optimize the commonly used method for the target protein of interest. The main steps include electrophoresis and blotting, where the proteins are separated according to size while they are migrating through a gel matrix, followed by a transfer of the proteins to an adsorbent membrane to create a replica of the original gel. We then utilize specific antibodies to detect the target protein. The technique is derived from DNA and RNA blotting and was named "Western blotting" to maintain consistency with the geographical naming tradition. We recommend a standardized methodology to obtain high-quality, reproducible, quantitative western blot data. (Taylor *et al.*, 2013; Kurien and Scofield, 2006). Western blotting analysis involves protein extraction, SDS-PAGE, and immunoblotting.

Transfection with siRNA

Transfection involves inserting foreign nucleic acids into cells, creating genetically altered cells. This process is a valuable method for examining gene and protein functionality and control. There are two distinct of transfection categories: stable and transient. Stable transfection integrates the introduced genetic material into the host genome, while transient transfection only temporarily expresses the introduced material. Transfection is used in various applications, such as gene therapy, siRNA knockdown, and protein production. The ideal transfection method should have high efficiency, low toxicity, minimal effects on cell physiology, and be easy to use and replicate *(Kim and Eberwine, 2010)*.

Small interfering RNA (siRNA), known also as silencing RNA, is a double-stranded RNA segment with various biological functions. Transfecting siRNA into cells can greatly aid gene silencing experiments, but the optimal method and transfection agent may vary based on the cell line used. RNA interference has been effectively demonstrated in many cells and tissues, where the knockdown of gene expression can result in partial or complete gene suppression. The length of siRNA is a crucial factor to control to avoid triggering an interferon response and causing apoptosis (*siRNA Transfection*, 2023).

The outcome of RNA interference (RNAi) experiments is contingent on the approach used to introduce siRNA. Transient or stable transfections can be used, but some cell types may require special transfection techniques. When designing siRNA, a library can help identify potential off-target effects, and the target site should have good specificity and avoid SNP or UTR regions (*siRNA Transfection*, 2023).
Determining optimal transfection parameters is important for successful siRNA experiments, and many factors such as siRNA concentration, cell confluence, and culture conditions should be considered (*siRNA Transfection*, 2023).

Lipofectamine RNAiMAX reagent is a proprietary product designed for the efficient delivery of RNAi or siRNA to mammalian cells. A recommended procedure is provided for transfecting RNAi or siRNA into human ASCs using Lipofectamine RNAiMAX. The reagent has broad activity, enabling maximum knockdown levels with minimal optimization. Key guidelines for transfection include using forward transfection, assessing transfection efficiency with Silencer Select siRNA, using 10 nM RNAi duplex and Opti-MEM reduced serum medium to dilute RNAi and reagent, avoiding antibiotics in media, testing serum-free media compatibility, and adhering to the broad range of cell densities and transfection reagent volumes for maximal activity (*Thermofisher – Invitrogen)*.

In the present investigation, optimization experiments were carried out to determine the most favourable conditions for siRNA transfection of LRRC8A. the experiments evaluated the impact of varying the concentration and duration of knock-down on the results.
Prior to conducting transfection experiments, a portion of the DMEM/F12 + FBS media, without the PenStrep, was taken out and stored at -20. The volume of PenStrep was then adjusted to 1% of the total volume of the remaining media.
There were three different types of transfection experiments performed. In the first experiment five petri dishes, each 100 millimeter in diameter, were seeded with 600,000 cells per dish to accommodate the various treatments. The two distinct siRNAs were tested against *LRRC8A* to determine the most effective one. The following samples were used:

- A control siRNA, #4390844 from ThermoFisher Scientific. The control is a random RNA sequence that is not complementary to the mRNA in the cells. This random RNA

sequence serves as a control for any transfection-induced effects on the cells, such as stress response.

- siRNA against LRRCA8 #1, p32107 from ThermoFisher Scientific
- siRNA against *LRRC8A* #2, p32109 from ThermoFisher Scientific
- a combination of siRNA against *LRRC8A* #1 and #2 to test for improved knockdown; and non-transfected cells as a control.

In the first experiment, the effectiveness of various siRNA against *LRRC8A* was evaluated. Upon analysis of the results, it was concluded that siRNA #1 demonstrated the most optimal effects, thereby leading to its selection for further use.
Building on the findings of the first experiment, the second and third experiments were designed to further validate the results by utilizing SAT cells and VAT cells, respectively.
These two experiments aimed to assess the efficiency of siRNA #1 in two distinct cell types, providing a comprehensive understanding of its performance and potential applications.
Six parallel runs were performed for each stimulation/experiment.
In the second and third experiments, 4 wells of a 6-well plates were seeded with 100.000 – 200.000 cells per well for various treatments (Figure 14). To accommodate two types of cells; SAT and VAT, 6-plates were used for each time course and the experiment was repeated 3 times for each cell type. Cells to be harvested at different times were seeded in separate plates. Of the plates, four were used for cell harvesting 4 different days, while the remaining plates were utilized for ORO staining on days 9 and 14.

To conduct the transfection procedure, an optimized protocol for pre-adipocytes using RNAiMAX transfections reagent was implemented as follows:

- The pre-adipocyte cells were seeded at a density of approximately 200,000 cells per well in a 6-well plate the day before transfection in a basal medium containing DMEM/F12, 10% FBS, and 1% PenStrep.
- The cells were ensured to be 30-50% confluent on the day of transfection.
- For transfection, 1.5 µl (20 µM stock, 30 pmol) siRNA was diluted in 250 µl Optimem and mixed by pipetting.

- Additionally, 5 µl Lipofectamine RNAiMax was diluted in 250 µl Optimem and a common dilution for all plates were prepared.
- The RNAiMax and siRNA dilutions were combined and mixed by pipetting and allowed to incubate for 20 minutes at room temperature.
- The medium in the wells was replaced with 2 ml of sterile-filtered medium without antibiotics.
- The transfection complexes were added dropwise to the wells.
- The medium was changed 5-6 hours after transfection or the next day to 2.5ml basal medium with PenStrep (Figure 15).

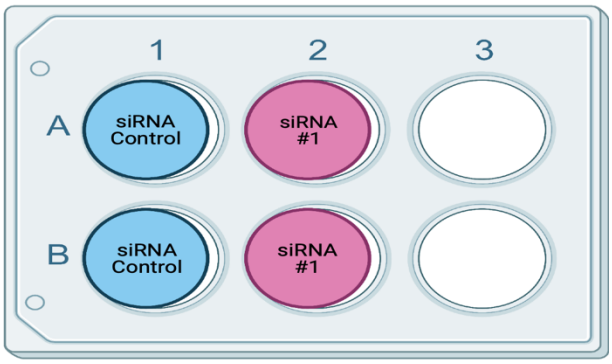

Figure 14 siRNA Treatment Layout in Wells - Created with BioRender.com.

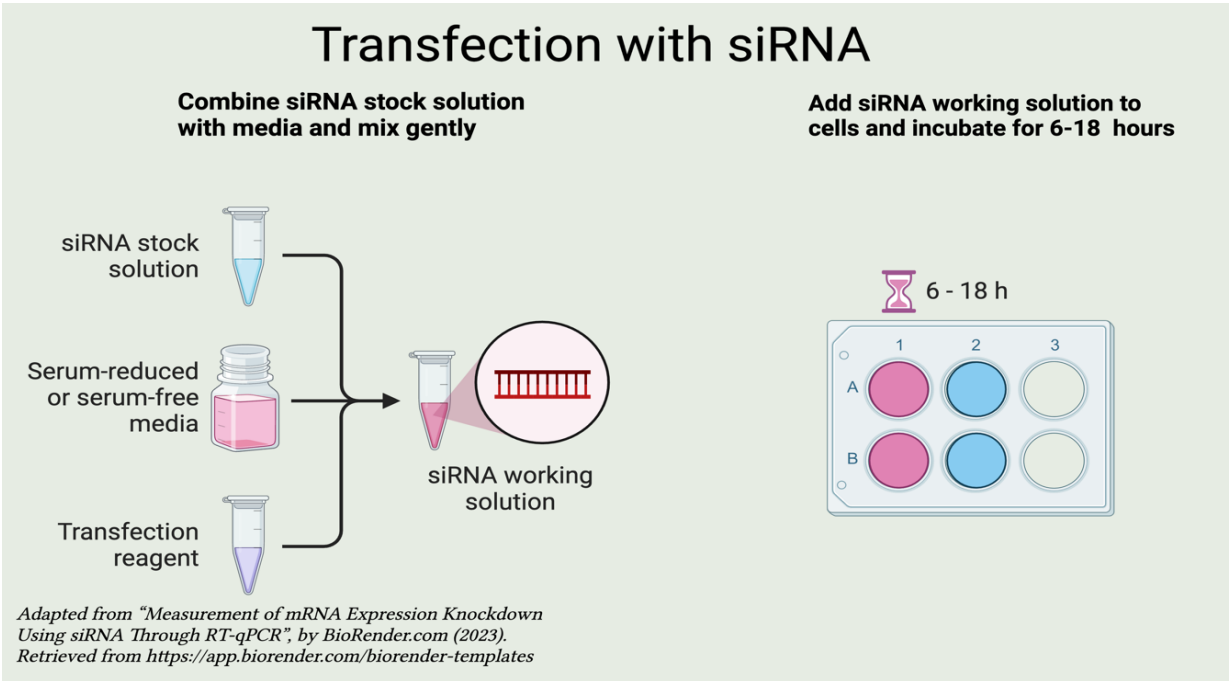

Figure 15. The 6-wells plate used in transfection and differentiation experiments. The figure was created with Biorender.com

Protein extraction

Protein extraction is the first step of western blot analysis. It requires breaking apart cells to extract their proteins, typically through mechanical disruption, detergents, enzymes, or other methods – before collecting and isolating them from other cellular components for further examination in western blot (Cox et al. 2011).

Typically, we separate protein mixtures by molecular weight using SDS-PAGE, and then electrophoretically transfer them onto membrane-like nitrocellulose or PVDF. Here, we probe them with a specific antibody targeting the protein of interest (Arunachalam and Sasidharan, 2021).

The versatility of RIPA buffer in extracting proteins from various cell fractions, such as membrane, nuclear, and cytoplasmic, makes it a favourable choice. Additionally, RIPA buffer's compatibility with follow-up assays further enhances its suitability (Marin *et al.*, 2019).

The following was the protein extraction protocol for SAT and VAT cells grown in 6-well plates/100 mm single Petri dishes. Preparations before the extraction are as follows: 10x RIPA buffer was diluted with distilled water to make 1x RIPA buffer. We prepared 1x RIPA buffer and added a protease inhibitor cocktail. Refer to ***Table #*** for the volume. We vortexed the mixture until the tablet dissolved. We kept the buffer on ice. The sonication is performed at 4 °C. The sonicator had an adapter for only six tubes, so we had to sonicate the samples in separate tubes. The maximum volume for sonication tubes was 300 µl. We kept a tabletop centrifuge at 4 °C. We also labelled a set of sonication tubes, three sets of protein low-bind tubes/1.5 ml Eppendorf tubes, and one set of 1.5 ml tubes for freezing (three tubes per stimulation type), along with a 96-place storage box, each marked with relevant information, name, and date.

We used cell scrapers, employing one scraper per type of stimulation. We placed the plates in a large Styrofoam box with ice.

Protocol for protein extraction was as follows: Previously snap-frozen plates were taken from the -80 °C freezer and immediately placed y on ice. 100/450 µl of cold 1x RIPA buffer was added directly to all plates/wells. The plate was rocked slightly to distribute the extraction buffer over the entire plate/well bottom the plates/wells were scraped thoroughly, and the lysate was

transferred to sonication tubes. 300 µl of lysate was added per sonication tube. The cell scraper and pipette tip were changed when switching between wells with different stimulation. The tubes were then shaken for 20 minutes at 700 rpm at 4 °C. SDS was added to achieve a final 1% SDS per tube, i.e., 300 µl = 15 µl of 20% SDS solution. Sonication was performed for 5 sets of 30 seconds ON/OFF (high) with the bioruptor. The Bioruptor Plus by Diagenode is a sonication device capable of processing multiple samples simultaneously while improving sample quality through precise temperature regulation. The device is beneficial for shearing chromatin and cell and tissue disruption. Before centrifugation, the lysates were transferred to new 1.5 ml protein low-bind tubes. The samples were then centrifuged at 4 °C for 20 minutes at 13 500 G. After centrifugation, the supernatant was transferred to a new set of tubes. For protein concentration measurements, 5 µl of each lysate was added to a separate set of tubes, and 315 µl of MQ water was added to achieve a 1:64 dilution. The lysate was aliquoted into volumes of approximately 200 µl per stimulation, i.e., 3 tubes per stimulation. The samples were snap-frozen and stored at -80 °C.

SDS-PAGE

Tris-glycine Sodium Dodecyl Sulphate Polyacrylamide Gel Electrophoresis (SDS-PAGE) is the most used strategy for electrophoretic protein separation in Western blot analysis. Prior to the SDS-PAGE procedure, the protein lysates need to be premixed with a sample buffer. The sample buffer is pre-added beta-mercatopethanol (produkt#/leverandør) freshly before usage and. since the buffer contains both SDS (a strongly anionic detergent) and beta-mercaptoethanol (a reducing agent) and the sample/buffer mix is boiled for 5 min/100 °C, it causes the proteins to be unfolded, denatured and bind to SDS within hydrophobic regions, resulting in a negative charge. The key feature of the procedure is that the amount of SDS that binds to the denatured proteins is roughly proportional to their molecular mass. This allows the highly negatively charged SDS-protein complexes to migrate directionally in the polyacrylamide gel based on polypeptide size (MacPhee, 2010).

The protocol for SDS-PAGE involved the following steps:

Preparations:

The bench was washed with alcohol, and new bench paper was used. The surface of the pipettes was wiped with alcohol, loading pipette tips, gel, and electrophoresis chamber and lid assembled. The samples, molecular weight marker (MWM). There were stored in a -20 °C freezer. 1 litre of 1x electrophoresis buffer was made by diluting 10x electrophoresis buffer with distilled water (100 ml concentrate + 900 ml distilled water). After thawing, all samples were vortexed and given a quick spin with the bench centrifuge to ensure that the samples were properly mixed. The wells were gently washed with distilled water from a spray bottle, making sure there were no gel remains left. The gel was placed in the electrophoresis chamber. The chamber was then filled with electrophoresis buffer to the indicated level in the chamber. Bubbles in the wells should be avoided, and the buffer was therefore poured gently. The samples were loaded with loading pipette tips as indicated on the loading set-up. The electrophoresis chamber was moved to the cooling room (4 °C). The constant voltage was set to 150 volts for 15 minutes. Slight bubbling was seen when the current was turned on. After 15 minutes, the voltage was increased to 200 volts. After the gels had finished running, after approximately 45-90 minutes dependent on the protein of interest, the power supply was turned off, and the entire tank was removed to a clean bench in the main lab. The gel was removed from the container, and a gel scraper/releaser was used on each side of the gel to open them. The plates were pressed apart, taking care not to damage the fragile gel. The gel was transferred to a small container containing pre-cooled blotting buffer. A small piece of the bottom right corner of the gel was cut off. The gel was allowed to equilibrate in buffer while gently shaking using the horizontal shaker.

Immunoblotting

Immunoblotting is a powerful technique that allows for the detection of proteins antigens immobilized on a protein-retaining membrane support, such as nitrocellulose or polyvinylidene fluoride (PVDF). This technique involves the binding of an antibody that specifically recognized the protein of interest exposed on the membrane. By combining protein separation via gel electrophoresis with immunochemical detection, immunoblotting can be used to determine the presence and steady-state level of the protein of interest in the sample, as well as its relative

molecular weight and distribution between cellular fractions. Electrophoretic transfer is commonly used to efficiently recover proteins from denser mesh polyacrylamide gels. The two main types of blotting systems used for electrophoretic transfer of proteins are “wet” and “semi-dry”. The wet system uses of a buffer-filled transfer tank, while the semi-dry system uses buffer-saturated filter paper sheets to conduct electricity (Litovchick, 2020).

Preparations went as follows:
2 litres of 1x blotting buffer were made: 200 ml 10x blotting buffer concentrate + 400 ml EtOH + 1400 ml MQ water. The entire flask of buffer was put in ice water in an ice bucket.
The scissors were washed with alcohol. The PVDF membrane was cut according to the template. The membrane covered the entire area of the gel. Tweezers to be used when necessary to handle the membrane. The membrane should also be cut at the right bottom corner. PVDF membranes were activated before they could be used for blotting. 3 chambers with space for membranes filled with, respectively, methanol (MeOH), MQ water, and blotting buffer. The activation involved a 3-step procedure: The membranes were activated by soaking them in methanol for a few seconds. It was made sure that the entire membrane was sufficiently soaked. When soaked, the membrane became shiny in appearance. The membranes were transferred individually into a container of distilled water and were rinsed thoroughly by shaking the container to ensure that the membranes were fully covered with water. They were then transferred into the blotting buffer and shaken. It was ideal for the membranes to remain in the blotting buffer for a while, till they were saturated with the buffer. This was seen best when the membrane sank into the bottom of the container, and the entire membrane was covered by the solution. If the PVDF membrane dried out, it needed to be re-activated. The membrane was allowed to equilibrate while gently shaking.

Wet blotting

For wet blotting, a cooling element should be used to prevent heat development. This can be achieved by freezing blotting buffer in a plastic container and using it in addition to pre-cooled blotting buffer.

The protocol was as follows:

The gel holder is opened, and the black side is placed down in the blotting tray. Cold blotting buffer is added to just cover the gel holder. A fiber pad is placed in the center of the black side of the cassette, followed by a blotting filter membrane that has been saturated with blotting buffer. The stack is then rolled with the rubber roller to eliminate any air bubbles, while holding it firmly with fingers on the side being rolled from, since air bubbles can prevent protein transfer to the membrane. The gel is then placed on the black side of the cassette using a gel applicator. A membrane is placed on top of the gel using forceps in one corner and a gentle grip in the opposite corner. It is centred directly on the gel with the notch at the bottom left and rolled gently with the rubber roller. A new blotting filter is then placed, rolled again gently with the rubber roller, and finally, a filter pad is placed on top and rolled gently again. The system must be constantly saturated with buffer. The cassette is closed by locking it with the white clip. The stack must not shift, and the cassette is placed in the electrode with the black side facing the black part of the electrode. The cassette is locked when it is a little way down in the electrode, and then pushed down so that it is covered with buffer. This process is repeated with cassette number two, and the cooling element is inserted. Ensured that the tray was filled with enough buffer to fully cover the gels and then submerged the entire tray in an ice bucket filled with ice water. The standard conditions for wet blotting were 100 volts for 60-120 minutes at a cold room temperature. While the blotting was running, a 5 % dry milk blocking solution for membrane incubation were prepared as follows:

Measured 5g of dry milk into a small flask and filled it with 100 ml of TBS-tween (tris-buffered saline) buffer. Added a stir bar and set the solution to stir on a magnetic stirrer. Heated the solution to denature the milk proteins. Filtered the solution into a new clean flask using a filter membrane and funnel. Cooled the solution on ice water.

After the wet blotting procedure was completed, the power supply was turned off and the lid was removed. The membranes were then transferred into appropriately labelled containers, and about 30 ml of 5% dry milk was added for blocking The containers were gently shaken to ensure even coating of the membranes. For gel staining, the membranes were placed in new containers containing Coomassie staining solution and shacked for some hours. After sufficient staining of the gels, they were rinsed/incubated thoroughly with water to remove excess staining.

Immunostaining

A specific antibody, which could be polyclonal or monoclonal, will bind to the target protein blotted onto a PVDF membrane. Any unbounded antibody was then removed by washing with TBS-tween. A secondary antibody, conjugated with an enzyme (typically HRP, or horse-radish peroxidase), was added to label the primary antibody. Finally, chemiluminescence was detected through a digital camera, such as LAS3000mini.

The protocol for immunostaining went as follows:
The membranes were blocked with 5 % dry-milk in TBS-t for minimum 1 hour and up to 2 hours, (depending on the type of antibody), at room temperature with gentle shaking. (However, alternative blocking solutions, including BSA or commercial blocking reagents such as Western blotting reagents from Roche (= 10x milk solution (casein) that is diluted to 1x). Washing was performed by immersing the membrane in TBS-tween, 20 mL each, and washing it twice for 5 minutes and once for 10 minutes under gentle shaking at room temperature. For incubation, the primary antibody was applied to the membrane and incubated overnight at 4 °C under gentle shaking. A 1:1000 dilution of the antibody in TBS-tween was typically used, and 10 mL of antibody solution per membrane per container.

For washing, the membrane was immersed in TBS-tween, 20 mL each, and washed twice for 5 minutes and once for 15 minutes under gentle shaking at room temperature. The membrane was exposed to the secondary antibody and incubated for 1 hour at room temperature under gentle shaking. The secondary antibody was typically diluted to 1:2500 in 5% dry milk in TBS-tween that had been heated and cooled and filtered. 10 ml of antibody solution per membrane per container was used. For washing, the membrane was immersed in TBS-tween, 20 ml each, and washed twice for 5 minutes and once for 15 minutes under gentle shaking at room temperature. To ensure optimal performance, the cooling system of the camera was activated at least 10 minutes prior. The Fujifilm machine, consisting of a CCD camera which captured images of the membranes from above, required a cool environment.
For the development process, the following items were required:
Transparent paper to cover the membranes. A development plate capable of developing 2/4 membranes simultaneously. A self-fluorescent substance for making the marker (250, 150, 100,

50, and 37 kDa bands were marked with a single dot, while 72 kDa and 25 kDa bands were marked with two dots).

To achieve development, a chemiluminescence solution called ECL prime was used, which was a mixture of solution A and B in a 1:1 ratio (3 + 3 ml). the containers were manually rotated to ensure the entire membrane was evenly saturated, and it was crucial to use a lid because the solution became toxic after mixing. Next, the membranes were incubated with the ECL solution while being gently shaken for a maximum of 5 minutes. Excessive incubation with ECL prime before transferring to the development plate could lead to signal saturation, as revealed by tests. Thus, for antibodies that produced strong signals, it was beneficial to incubate them for a shorter duration (1 minute). Once incubation with ECL was complete, the membranes were transferred to the development plate and centred as much as possible. They were covered with transparent paper, and care was taken to ensure no air bubbles were present between the membrane and the paper. Any ait bubbles were gently removed by pushing them with a finger, but care was taken not to scratch the membrane.

The molecular weight marker (MWM) was labelled using a self-fluorescent probe, and dots were placed on the transparent paper using a loading pipette. It was noted that small dots produced a strong signal during development. Initially, short exposure times (20-30 seconds) were used, followed by 1 minute, 5 minutes, and 15-20 minutes, with adjustments made based on the initial signal strength. ECL prime, a detection reagent that produced a signal for an extended period, worked optimally within the first 30 minutes. Although the signal persisted after this time, prolonged exposure was required, and the signal became increasingly indistinct. The images were saved as both TIFF and IMG (Figure 16).

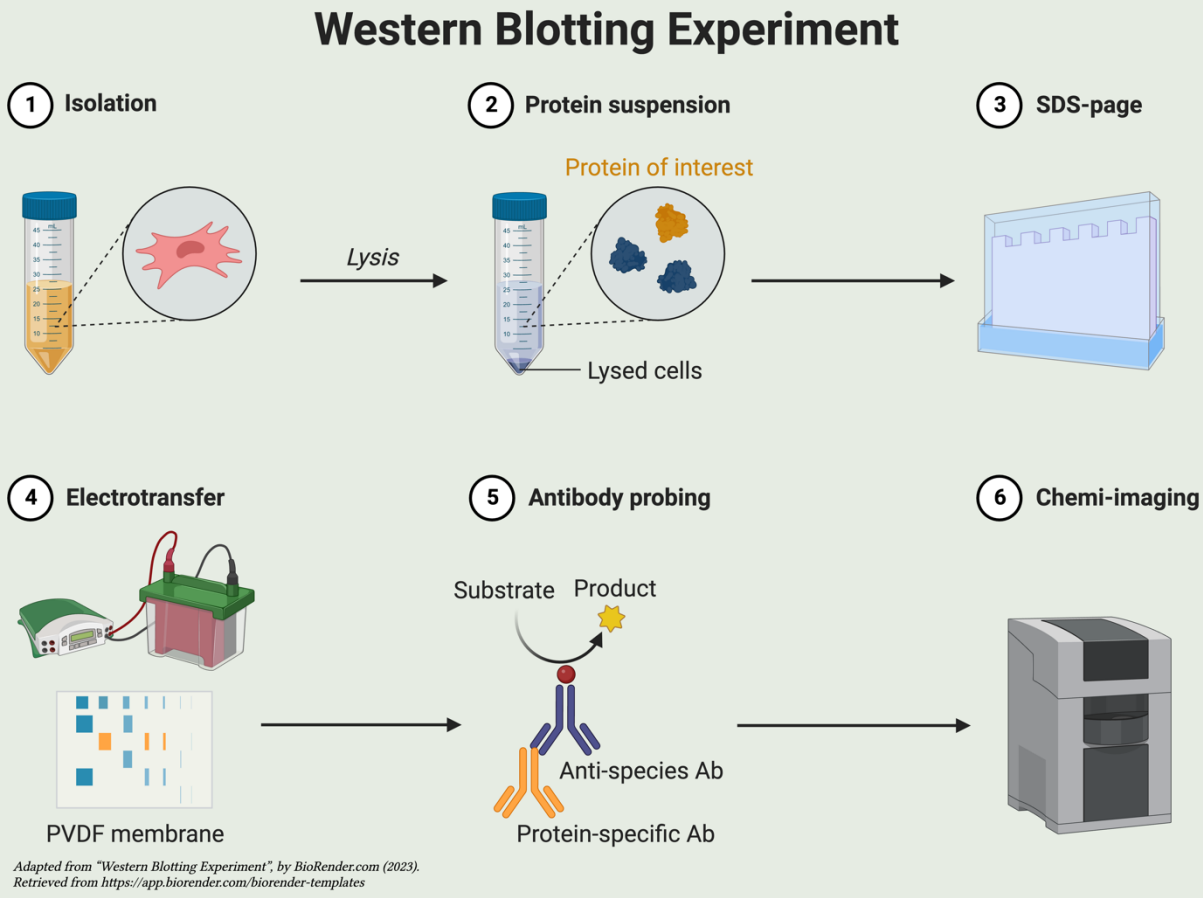

Figure 16 Steps in a Western Blot Analysis - Adapted from "Western Blotting Experiment", by BioRender.com (2023). Retrieved from https://app.biorender.com/biorender-templates.

Semi-quantification of western blotting results

Semi-quantification of western blotting results is used to estimate relative protein amounts present in samples. This technique compares target protein band intensities against those from reference proteins or loading controls. While not precise, it gives an approximate indication of relative levels across various samples. Although not measurements, this approach provides a reliable indication of protein concentration differences. Densitometry software measures intensity differences across individual protein bands on a blot (Gilda & Gomes, 2015; Taylor et al., 2013).

Protein Concentration Measurement Using BCA Assay and ELISA Plate

The procedure involved preparation of samples, preparation of BCA reagent, performing the assay, and measuring the absorbance.

The proposed approach utilized a patented, detergent-compatible bicinchoninic acid (BCA) formulation for the colorimetric detection and quantitation of total protein. In an alkaline environment, the detection reagents BCA reacts with Cu +2, which is reduced by protein, resulting in the formation of Cu +1. The reaction between two molecules of BCA and one Cu +1 ion produces a water-soluble, purple-coloured complex that has a strong absorbance at 562 nm, which is linearly correlated with increasing protein concentrations (O'Callaghan and Pierce. Rockford, IL., 2017).

Pierce, Diagen and GE Healthcare each offer protein measurement kits suitable for different concentrations ranges, depending on expected protein concentrations. The Micro BCA proteins assay kit can measure samples with concentration levels between 0.5 – 20 µl/ml while their BCA protein assay kit measure greater ranges (20 – 2,000 µl/ml and 5 – 250 µl/ml).
The samples were assembled in a 96-well plate using Thermo Fisher Scientific kit #23235 (Figure 17). Each standard and sample were measured in triplicate (up to 24 samples) for accuracy.
In preparation for the experiment, both the samples/standard and the plate were kept at 4 °C, and an incubator cabinet was set to 37 °C.
Diluting samples at 1:64 by mixing 5 µl of protein lysate with 315 µl of MQ water created a 1:64 ratio. Following dilution, all samples were mixed by vortexing and then spun down promptly. The same sample was added in triplicate as indicated in the overview, using inverse pipetting and the same tip for each application. If ensure of the technique, regular pipetting was employed instead, and the tip was changed for each application.
The samples were kept chilled on ice while BCA reagent mix was prepared and added individually using a multi-channel pipette (8 channels). After adding the BCA solution, the plate was sealed with a sealing film and then incubating at 37 °C for two hours. Once equilibrated to room temperature, absorbance values were obtained using ELISA plate reader at 562 nm and blank values subtracted. Then, the correct dilution factor entered. Final concentration values were calculated in µg/µl and obtained by dividing by 1000 in Excel. For BCA calculations, samples and BSA standards were further diluted 1:1 and incubated on the plate under gentle agitation before calculation results.

The BCA reagent mix was prepared and consisted of:

80 µg/ml	1000 µl 0.2 mg/ml (stock) + 1500 µl MQ water
40 µg/ml	500 µl 80 µg/ml + 500 µl MQ water
30 µg/ml	150 µl stock + 850 µl MQ water
20 µg/ml	500 µl 40 µg/ml + 500 µl MQ water
10 µg/ml	500 µl 20 µg/ml + 500 µl MQ water

Table 1 Standards of BSA

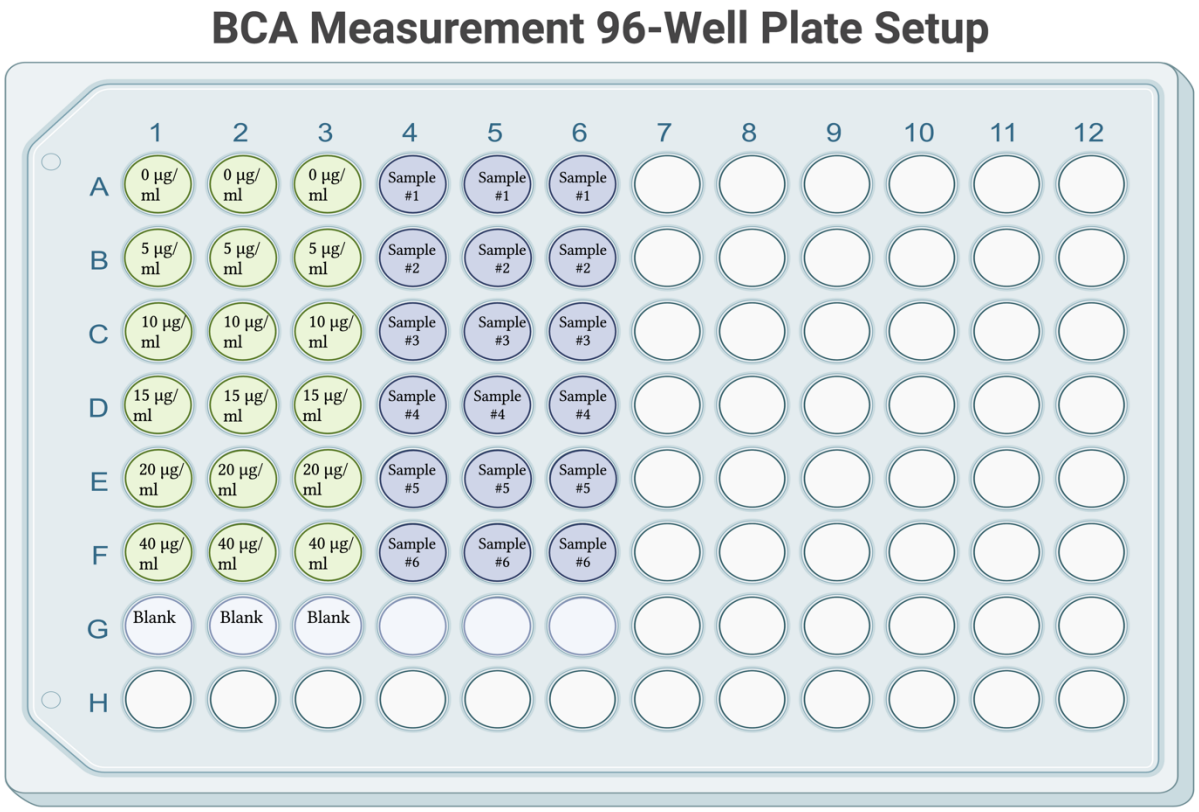

Adapted from "Editable 96-Well Plate", by BioRender.com (2023). Retrieved from https://app.biorender.com/biorender-templates

Figure 17 96-Well Plate Layout for BCA Assay

Adipogenic differentiation

Adipose tissue growth encompasses adipocyte hypertrophy and adipogenesis from precursor cells. A comprehensive understanding of adipocyte differentiation and gene cloning has provided invaluable insights into adipose tissue growth, which is crucial for devising effective obesity control strategies. The temporal regulation of gene expression during the differentiation of preadipocytes into adipocytes results in the accumulation of triglycerides. Agents such as dexamethasone, methylisobutylxanthine, and high concentrations of insulin can expedite the differentiation process (Gregoire, Smas and Sul, 1998).

The adipogenic differentiation medium; a mixture of 50 mL basal medium, 50 µL IBMX (0.5mM), 50 µL Dexamethasone (1µL), 50 µL Indomethacine (0.2mM) and 50 µL insulin (10µg/ml) was prepared and filtered through a 0.2 um sterile filter prior to use. (Refer to ***Table #***).

The adipogenic differentiation of pre-adipocytes was carried out as follows:
Pre-adipocytes were plated at high confluency, with 125.000 cells/cm^2 in basal medium (excluding bFGF). The next day, the adipogenic differentiation medium was added to the cells after they reached full confluency, which is a key for optimal differentiation. The medium was changed every 3-4 days. On day 9 and day 14, cells were collected for Oil Red O staining, with formaldehyde fixation. RNA extraction and isolation were performed on cells collected on day 0, 1, 3 and 9 (Figure 18).

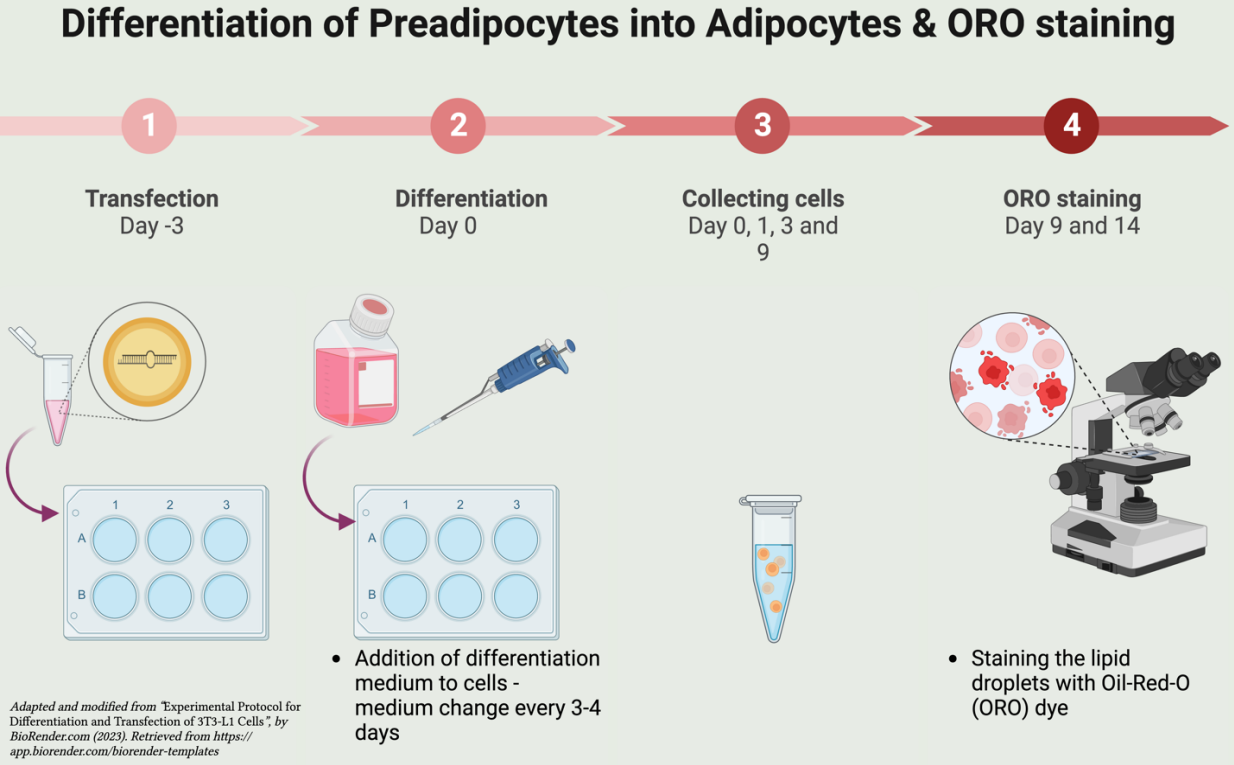

Figure 18 Adipocyte Differentiation & Lipid Staining - Adapted and modified from "Experimental Protocol for Differentiation and Transfection of 3T3-L1 Cells", by BioRender.com (2023). Retrieved from https://app.biorender.com/biorender-templates.

RNA Extraction and mRNA Quantitation

RNA extraction is a technique for isolating and purifying RNA from biological samples to examine gene expression and function further. The process typically includes cell lysis, separation from other cell components and isolation/purification. Quantifying messenger RNA (mRNA) in samples is an analytical procedure to estimate its amount, used to assess gene expression levels and cell functions and responses to stimuli. Real-time PCR or next-generation sequencing techniques are often employed for this task.

The protocol for the extraction were as followed: at first, we removed media from cells and washed them with PBS and ensure that we removed all media and PBS. Under a cell culture hood, we added 350 µL of QIAzol to each well and collected the lysates using a cell scraper. After that, we moved these mixtures into our QIA shredder spin column, located in 2 ml collection tubes. We then centrifuged these at full speed at room temperature. Following centrifugation, we let them rest on a benchtop for three to five minutes to allow for nucleoprotein complex dissociation. After adding 70 µL of chloroform to our lysates, we sealed and vortexed for 15 seconds before allowing it to sit at room temperature for several minutes before centrifuging for 30 minutes at 4 °C at 12.000g for phrase separation. Finally, we transferred the

aqueous phase with RNA into another tube before mixing it with 70% ethanol for final processing.

Transferring our solution into a RNeasy mini spin column, we then centrifuged it for 15s at >8000g (>10.000rpm). Following multiple washes with buffer RW1 and buffer RPE – with centrifugation occurring after every wash step – it was place into a new collection tube before centrifuging at full speed to remove residual ethanol before incubating at room temperature before further centrifugation to elute our RNA.

At this step, we measured RNA concentration by using 1 µL volume, using the NanoDrop Fluorospectrometer from Thermo Scientific. After assessing RNA concentration, we allocated the necessary amount for cDNA synthesis. Any excess material was stored at -80 °C until further use.

cDNA synthesis

Second strand DNA (cDNA) synthesis is a process used for creating complementary DNA libraries, sequencing, and cloning. This involves synthesizing a complementary strand to an existing single-stranded template using DNA polymerase I and primers with 3'-OH groups to start synthesizing sDNA. Subsequent use in downstream applications provides for more stable double-stranded molecules with reduced degradation rates (Kennedy et al.2015; Lee et al.2020).

In conducting the cDNA synthesis protocol, we began by utilizing an amount of RNA that we extracted before, typically 1 µg. In preparing the cDNA synthesis master mix, we incorporated several components, as shown in table # …

During the cDNA synthesis process, we kept cDNA synthesis reagents on ice. We prepared a 1.5 ml Eppendorf tube to hold the MasterMix. We calculated the required volume of MasterMix based on the number of the samples, creating an amount sufficient for X+2 samples. Upon preparing the MasterMix, we added 10 µL of it to the RNA samples, that we had already diluted. The reverse transcriptase was only taken from its refrigerated storage when we needed to add it to the MasterMix and was promptly returned right afterward. We thoroughly mixed the MasterMix each time we drew a volume from it using a pipette. We then mixed the MasterMix solution with the RNA samples by pipetting up and down. the samples were ready for the machine, and we spun the samples before putting then into the Mastercycler X50s machine by Eppendorf (Figure 19).

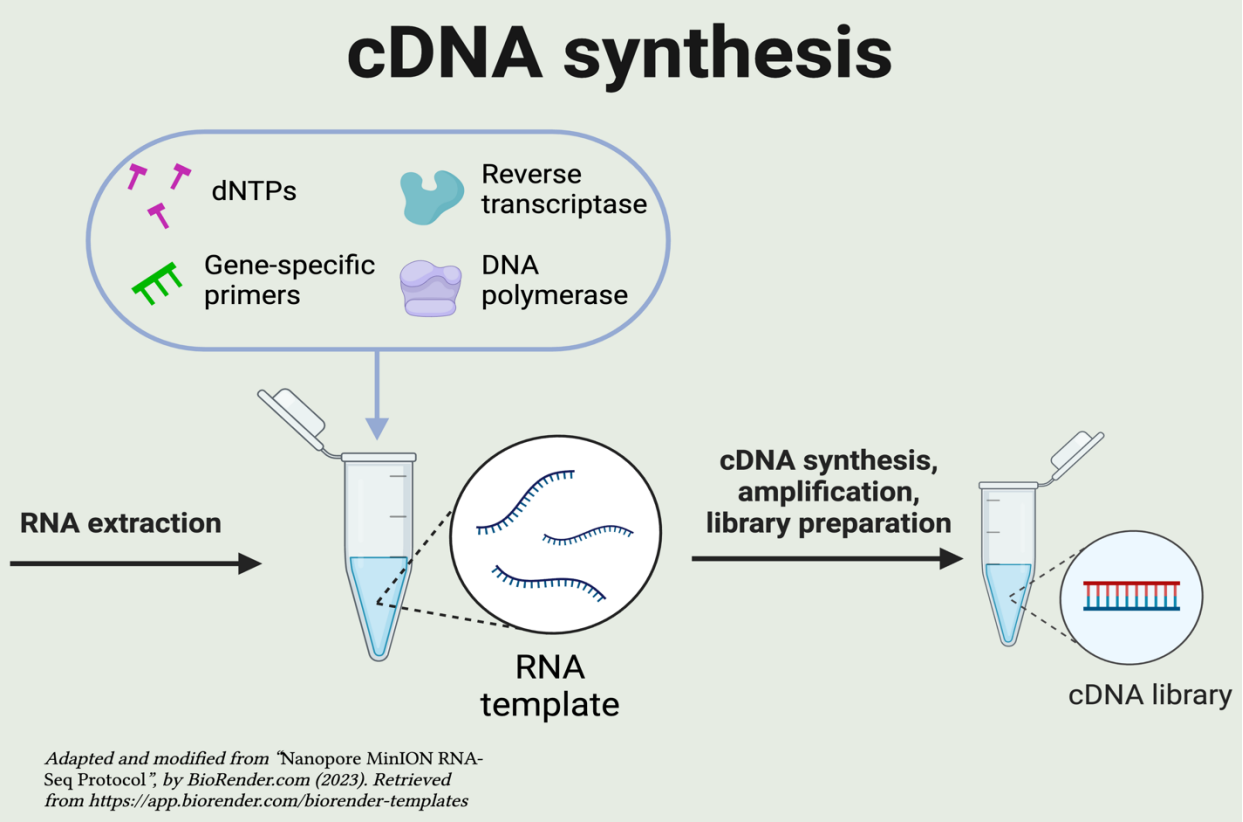

Figure 19 cDNA Synthesis from RNA Process

RT-qPCR

Realtime- quantitative reverse transcription PCR (RT-qPCR) is an invaluable tool that enables the detection and quantification of specific nucleic acid sequences – most often mRNA – with samples. Real-time tracking provides monitoring of this amplification during PCR cycles and provides both qualitative (presence or absence) and quantitative (amount) information. RT-qPCR's combination of sensitivity, specificity and wide quantification range make it a versatile method for gene expression analysis, diagnostics, and the detection of low abundance RNA target (Derveaux et al., 2010; Whale et al., 2020).

Quantitative PCR we conducted using 96-well plates and the cDNA samples synthesized earlier. We started by marking the Eppendorf tubes with sample information and diluting the cDNA 1:10 by adding 180 µL nuclease-free water and 20 µL cDNA to each tube. We prepared primer dilutions, which were stored at a common concentration of 100 µM. we created 5 µM dilutions

for each target, pooling the ditions of forward and reversie primers. This required a total volume of 200 µL, comprising 10 µL of forward primer, 10 µL of reverse primer, and 180 µL of nuclease-free water. The primers targeted mRNA for PPARG, CEBPA, FABP4, and the housekeeping gene PPIA. All primers had been previously validated for specificity and PCR efficiency. We then prepared the MasterMix as per the volumes provided in table # … After adding all the reagents, we mixed them thoroughly by pipetting, avoiding forming and refraining from vortexing. In the next step, we used the multistepper pipette, which is beneficial when pipetting the MasterMix. We first added 8 µL of MasterMix to the bottom of each well, and then applied 2 µL of cDNA for the side of the well, which made it easier to identify whether we had added the sample if there was any doubt. We included non-template control (NTC) for each primer pair to monitor for contamination of reagents. Final step, we ran the qPCR on the Quantstudio 6 pro, following a standard qPCR program that included a melt curve step at the end.

Statistical methods and Software

This thesis employed several statistical techniques to organize and gain insights from a dataset. Initial cleaning and organizing were carried out via Microsoft Excel as it is an accessible platform to prepare information for further examination. For statistical analysis purposes and visual presentation of the data, we used RStudio, a statistical computing and graphics software.

In order to assess the effectiveness of reducing the *LRRC8A* gene and its impact on indicators of fat cell development, we employed statistical methods. The main technique used to compare gene expression between the control group (siCtrl) and the group with the reduced *LRRC8A* (siLRRC8A) was the Student's t-test. This test is well suited for comparing means of two groups that are independent. By using this t-test we obtained p-values that indicate the likelihood of observed differences in gene expression occurring by change. When these p-values were below 0.05 it suggested a difference between the two groups supporting our hypothesis that reducing *LRRC8A* has a measurable effect. Additionally, to ensure our findings are reliable and to assess their significance we conducted a power analysis. power analysis is crucial during study design as it helps determine the sample size needed to detect an effect of a certain magnitude with confidence. To calculate the effect size for the power analysis, we employed Hedges g, which is

a version of Cohens d that accounts for sample size discrepancies. Hedges g is especially valuable when dealing with sample sizes as it corrects for any biases that may arise in such cases. By applying Hedges g in our power analysis, we were able to gain an understanding of the impact and direction of effect on adipocyte differentiation resulting in knockdown. When presenting our findings we combine p-values with fold change values. The fold change provides a measurement of gene expression alteration while the p-values and power analysis add context enabling to draw conclusions about their reliability and relevance, from both statistical and biological standpoint. This comprehensive approach ensures that our findings are not only statistically significant but biologically meaningful. RStudio were integrated to ensure an effective statistical analysis that produced precise results, which is essential in producing robust findings from this investigation.

Results

The following parts were optimized:

- The effect of these two different siRNAs, siLRRC8A #1 and siLRRC8A #2.
- The time course with the siRNA that worked the best, performed on SAT and VAT.

The evaluation of *LRRC8A* knock-down in preadipocytes derived from SAT and VAT part included:

- Efficiency of gene knock-down. Relative expression and fold change of LRRC8A.
- Pictures from cell differentiation – to be included in the appendix part?

In our study we extensively examined the levels of protein breakdown in our samples. We conducted protein extraction on cell pellets with three samples containing one million cells each and three samples containing two million cells each. Protein concentrations were as shown in the Table 2**.**

Sample	Protein concentration (µg/ul)
#1, SAT, Protein lysis (1 mill cells)	1.0
#2, SAT, Protein lysis (1 mill cells)	0.8
#3, SAT, Protein lysis (1 mill cells)	0.8
#4, SAT, Protein lysis (2 mill cells)	1.3
#5, SAT, Protein lysis (2 mill cells)	1.4
#6, SAT, Protein lysis (2 mill cells)	1.4

Table 2

Our primary objective was to evaluate how well the antibody ab254389 (siLRRC8A #1) purchased from Abcam performed compared to its competitor, the antibody #24979 (siLRRC8A #2) from Cell Signalling. Therefore we have decided to incorporate the Abcam antibody siLRRC8A#1 into our experiments. Additionally, we conducted tests using three different amounts of protein lysate to identify the optimal Western Blot conditions; 10, 20 and 30 µg to detect LRRC8A through immunolabelling. Our main objective was to select a concentration that would produce the best results while taking full advantage of resources available and permitting for meaningful analysis of data.

LRRC8A Protein Detection Through Western Blot

To measure the efficiency of different antibodies at recognizing LRRC8A protein, we conducted a Western Blot analysis. Our aim was to compare binding affinity of two distinct antibodies towards the LRRC8A protein. For this experiment we began by loading 3 replicate wells with the antibodies as well as wells marked MWM (10 µg), indicating the standard used in the Western blot.

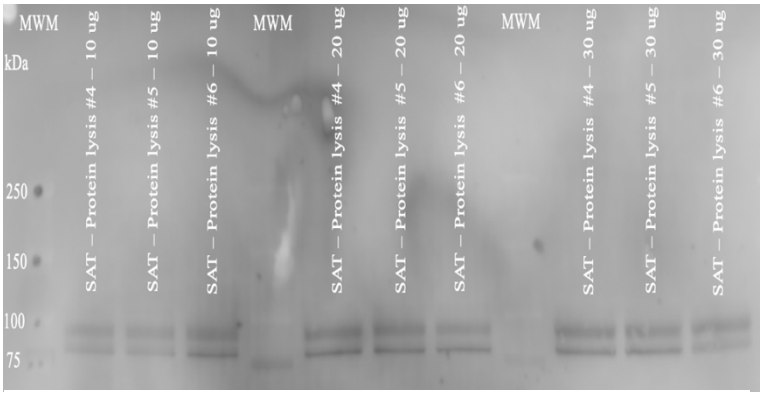

Figure 20 Western Blot Analysis of LRRC8A using Old Antibody #24979 from Cell Signalling

When captured at 90 seconds this image revealed faint lines which indicated weaker affinity of this antibody (#24979) from Cell Signalling (Figure 20). This may happen due to a weak affinity of the #24979 antibody towards the LRRC8A protein. In contrast, the second Western blot analysis focused on samples with lower protein **(**Table 4**)** to test the new antibody ab254389 from Abcam and showed much stronger bands despite having lower protein concentrations that Cell Signalling's antibody's Western blot analysis performed earlier (Figure 21). Its increased clarity underlines both potential of this new antibody. This suggests that the new antibody ab254389 exhibits an affinity for *LRRC8A* and a higher specificity, enhancing its detection capabilities. This finding indicates that this new antibody is more potent and can deliver reliable results during Western Blot analysis.

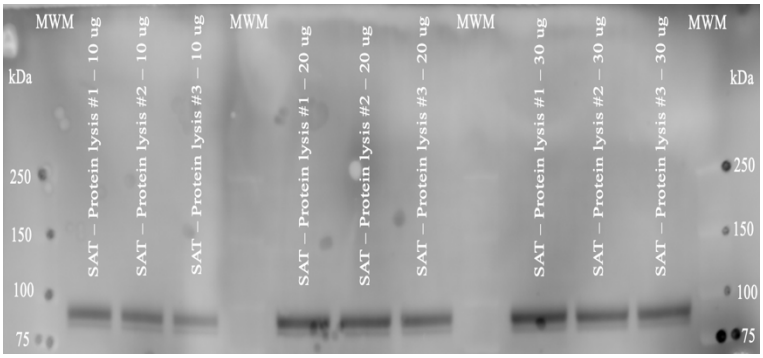

Figure 21 Western Blot Results for LRRC8A Using the New Antibody ab254389 from Abcam.

Optimization of conditions for siRNA knockdown using Western Blot

Next, we conducted an intensive 72-hour analysis using Western Blot. This involved scrutinizing SAT cells under various conditions as seen in figure X. Our methodology involved comparing cells treated with siCtrl, siLRRC8A #1 + #2 (two siRNA treatments combined), siLRRC8A #2 as well as a non-transfected group as a control. For each comparison group that received treatments; its untreated counterpart served as baseline measurement. Cell cultures examined over a 24-hour interval did not exhibit significant morphological changes. Consistency in cell morphology, density and confluence was observed across treated and non-treated groups, signalling healthy growth. For definitive conclusions to be reached, we further quantified and compared with additional experiments. The stability of non-transfected control cells provides evidence of their suitability as baselines to evaluate impactful treatments on cell morphology (Figure 22).

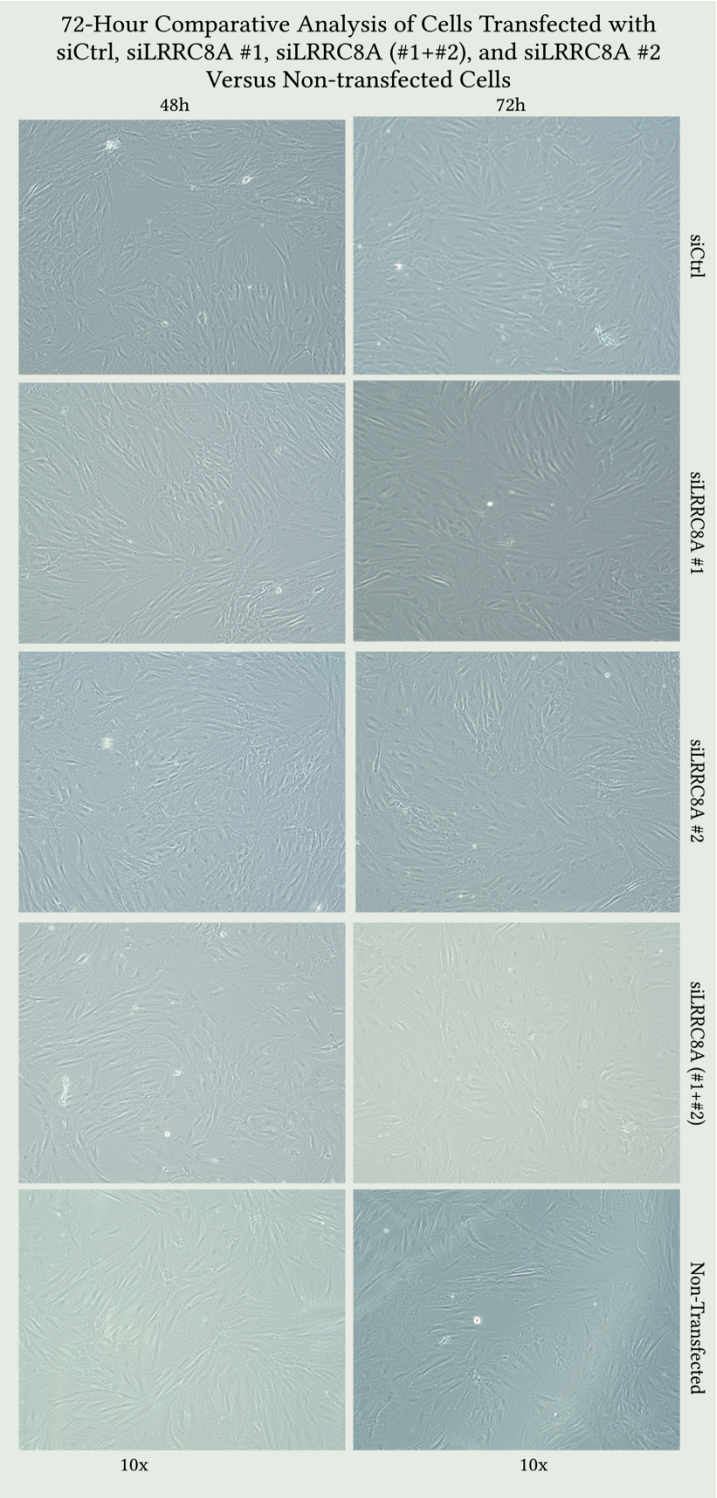

Figure 22

Western blot experiment normalized LRRC8A expression against Actin and Lamin (Figure 23), which are stable across cell types and experimental conditions and serve as controls (Johnson, 2012). Actin regulates cell structure, motility, and integrity. Its stable expression has made it a reference gene in many studies (***Beta Actin and GAPDH: The importance of Western blot loading controls-new reference needed here***). Lamin, a nuclear lamina structural component, is also a standard control because of its consistent expression levels (Johnson, 2012; Bio-Rad). These two control proteins account for experimental variability, such as cell number, total protein amount, and Western Blot transfer (Johnson, 2012; Bio-Rad). LRRC8A expression normalized to these two controls allows is to ensure the robustness of our results and minimize experimental artifacts, and that any observed variations in *LRRC8A* expression are not due to errors (Johnson, 2012).

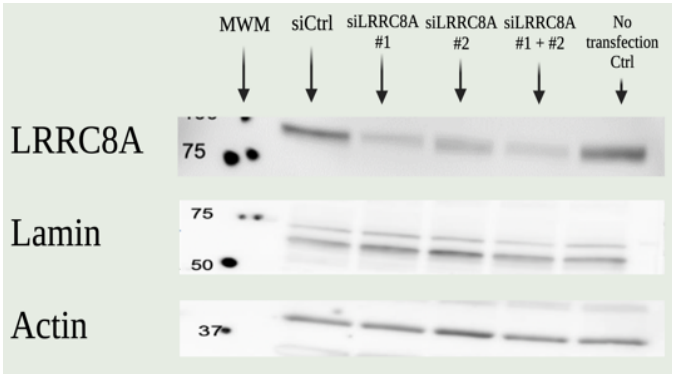

Figure 23 Quantitative Western Blot Analysis: LRRC8A Knock-Down Verified with Actin and Lamin

Examining the blot by starting with LRRC8A's siCtrl we can see bands on the blot (figure #). These bands indicate the presence of the protein. The clarity and sharpness of these bands suggest that the transfer process during blotting was successful. Both siRNA treatments indicate that they have some degree of effectiveness in reducing the expression of LRRC8A protein. The band intensity in the siLRRC8A #1 lane appears lighter than that in the control lane suggesting a reduction. Similarly, in the siLRRC8A #2 lane there is a decrease in intensity. These variations highlight that each individual siRNA treatment has an effect on knockdown. Considering the lane where we combined siLRRC8A #1 + #2 treatments, the band is fainter, indicating that using both siRNAs together enhances their knockdown effect. On the other hand, the "No transfection Ctrl" lane shows the natural expression of LRRC8A serving as a reference point to evaluate the effectiveness of the siRNA treatments (*Controls for RNAi experiments | Thermo Fisher Scientific*).

As mentioned before, we used Lamin and Actin blots as a control to ensure loading. The Lamin observed bands on this blot are well defined and align with the expected weight indicating transfer and antibody specificity (Figure #). However, slight variations in intensity can be observed in the Actin blot suggesting differences in loading or transfer efficiency between samples (Figure #). The findings of this experiment suggest the need for further optimization, which involved investigating protein transfer efficiency and antibody specificity, in our next Western Blot experiment.

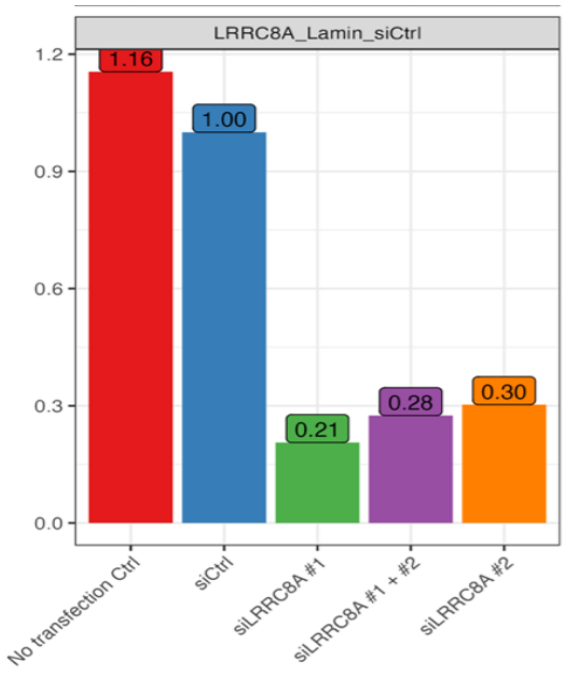

Figure 24 LRRC8A Expression After siRNA knockdown Compared to Lamin

The following figures shows the levels of expression for the protein LRRC8A compared to the proteins Lamin and Actin. Figure 24 displays the "No Transfection Ctrl" with LRRC8A expression at 1.16 as its baseline expression against which siRNA effects are assessed – validating normal levels for this cell type (Rubino *et al.*, 2018). A non-targeting siCtrl serves as a control during transfection processes while siLRRC8A #1 and #2 treatments reduce expression to 0.21 and 0.30 respectively to demonstrate effective gene knockdown; when combined together (siLRRC8A #1 + #2) similar reduction were observed (0.28), possibly due to either reaching maximum knockdown efficiency or competition for RNA induced silencing complex (RISC) mechanisms (Tanudji *et al.*, 2010).

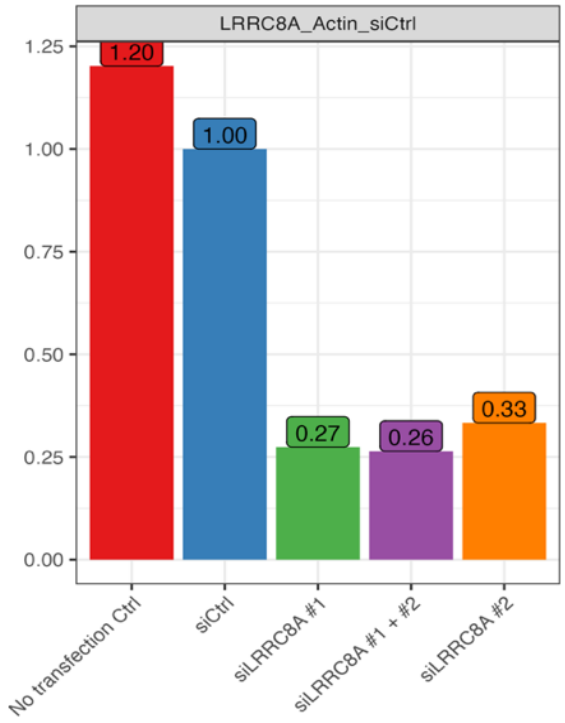

Figure 25 LRRC8A Expression After siRNA knockdown Compared to Actin

Figure 25 displays normalized levels of LRRC8A relative to Actin. The “No transfection Ctrl” has an initial baseline level of 1.20 while siCtrl doesn’t target any genes and maintains it at 1.00. siLRRC8A #1 treatments demonstrated siRNA efficacy by decreasing expression by 0.27, 0.26, and 0.33 respectively confirming siRNA efficacy while showing which siRNA #1 treatments works most effectively when combined together; likely due to the RISC binding competition combined siRNAs don’t significantly enhance knockdown results guiding future gene silencing optimization efforts. This study demonstrated that siRNA treatments successfully decreased expression of the LRRC8A gene compared to control levels. A non-targeting siRNA served as a control to verify that any observed knockdowns are indeed specific to siRNA treatments. Adding multiple siRNAs did not further silence gene expression suggesting competition within the RNA interference pathway and an upper limit for maximum knockdown efficiency.

Assessing The Impact of LRRC8A Knockdown on VAT Cells Through siRNA Transfection Study

This experiment sough to measure the efficacy of two siRNAs, siLRRC8A #1 and siLRRC8A #2, individually and combined on VAT cells morphology and LRRC8A protein suppression. Transfection followed by Western blot analysis was utilized to gain an insight into how gene knockdown affects cell chape and protein expression levels, using Actin as an endpoint control for normalization purposes.

The series of microscope images in Figure 26 displayed illustrated the comparison of VAT cell shapes following the administration of treatments, against a control group that did not receive any treatment. The cells treated with control siRNA display an elongated shape with density indicating regular growth patterns. On the other hand, cells transfected with siLLRC8A #1 exhibit changes in their shape potentially due to gene suppression affecting cell adhesion and possibly leading to cell death or altered progression through the cell cycle. When both siLRRC8A # 1 and #2 are combined, a similar change in cell shape is observed. It appears pronounced suggesting a possible additive or synergistic effect resulting from the combined siRNA treatments. Additionally, cells treated with siLRRC8A #2 exhibit shapes compared to the control group; however, this effect seems slightly less severe indicating either different target sequences or less effective gene suppression. Finally, non-transfected cells are included as a

reference point, for comparison, demonstrate the fibroblast-like shape expected in healthy adherent cells that have not undergone any treatment.

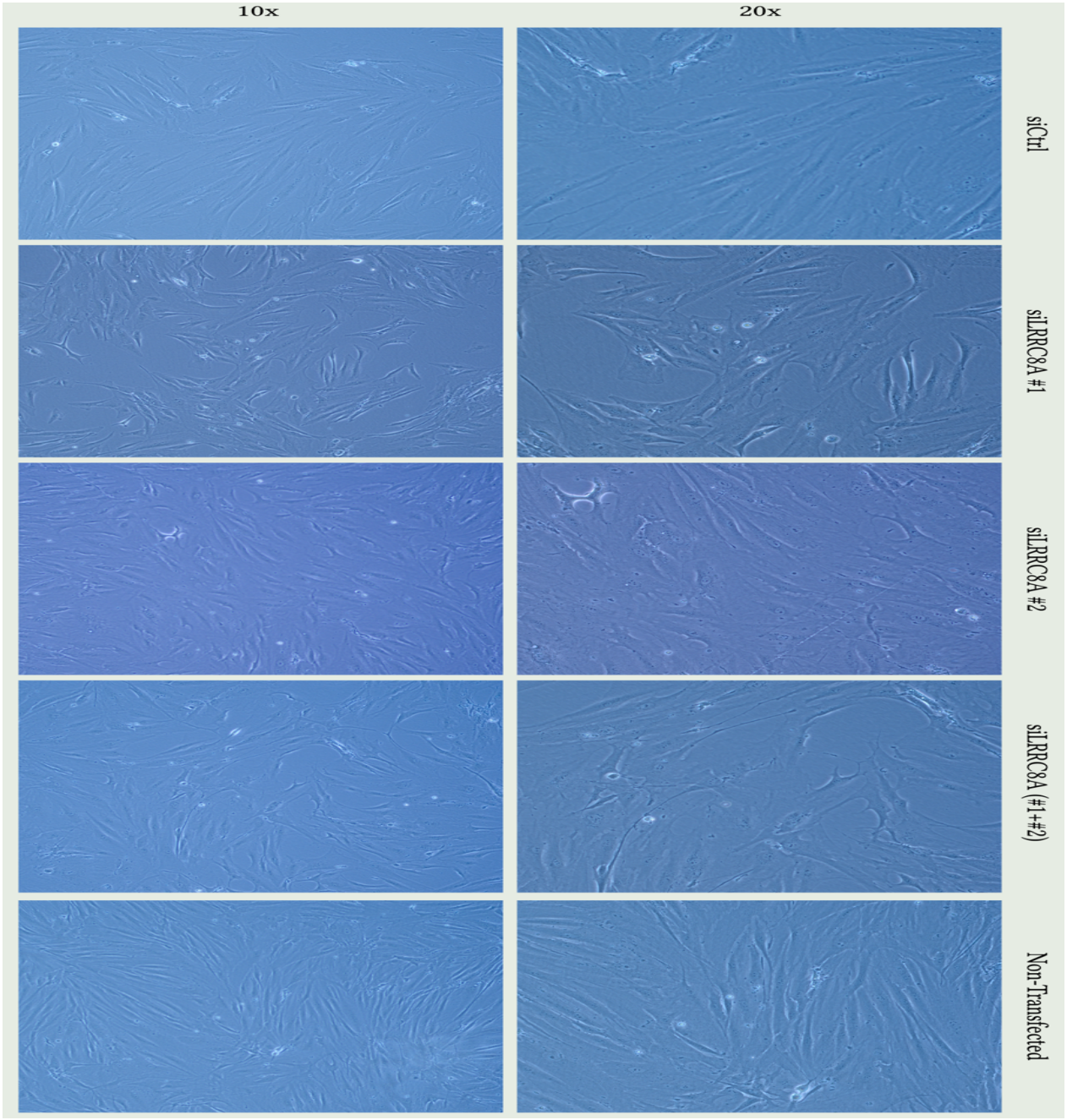

Figure 26 72-Hour Comparative Analysis of Cells Transfected with siCtrl, siLRRC8A #1, siLRRC8A (#1+#2), and siLRRC8A #2 Versus Non-transfected Cells.

Figure 27 shows the results of the Western Blot experiment. Comparing the bands from the siRNA treated samples with those from the control group reveals a decrease in LRRC8A levels after knockdown has been achieved successfully. Furthermore, the Actin bands patterns indicate loading across all samples were successful.

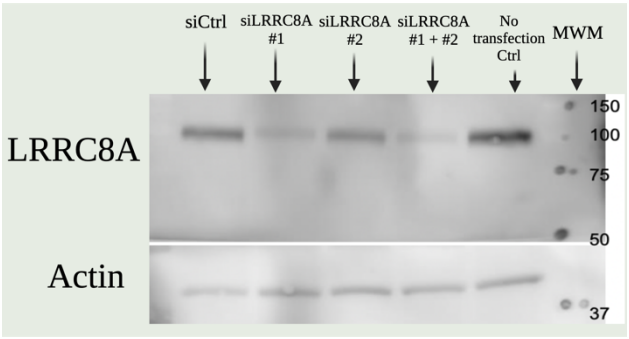

Figure 27 Quantitative Western Blot Analysis: LRRC8A Knock-Down Verified with Actin

Figure 28 presents a bar graph of normalized ratio of LRRC8A expression to Actin. The No transfection Ctrl group shows a ratio of 0.60 indicating the baseline expression level. The siCtrl group has a ratio of 1.00 serving as a reference for assessing transfection efficiency. The siLRRC8A #1 and siLRRC8A #1 + #2 bars demonstrate reduction with ratios of 0.13 and 0.11. on the other hand, the siLRRC8A #2 bar shows a significant reduction at 0.41 indicating that the effectiveness of knockdown varies among the different siRNA treatments.

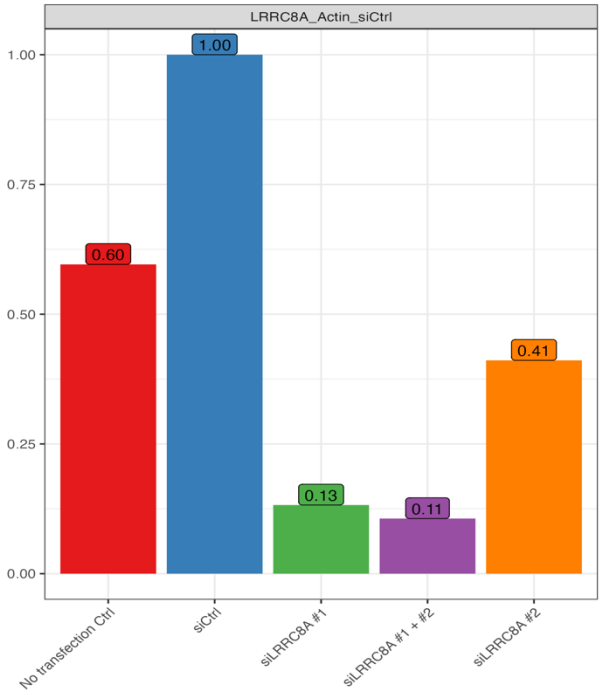

Figure 28 A Western Blot Quantification Analysis (WB233) to Validate LRRC8A Knock-Down by siRNA Transfection, Using Actin Control.

A Time-Course Study to Assess of LRRC8A Knockdown Stability Over Time on SAT

This transfection experiment was designed to assess the duration of LRRC8A suppression in SAT cells after transfection, to confirm its stability and the sustained knockdown for later experiments.

Figure 29 displays a collection of cell culture wells captured at 10x over a span of 10 days. It compares cells that received a control siRNA with cells that received an siRNA specifically targeting LRRC8A. The cells density appears similar in both conditions. However, as time progress the treated cells seem to be tightly packed suggesting an impact on cell growth or viability. This visual comparison provides insights into the effects of reducing LRRC8A through knockdown on cell behavior although further confirmation using other methods like RT-qPCR were conducted.

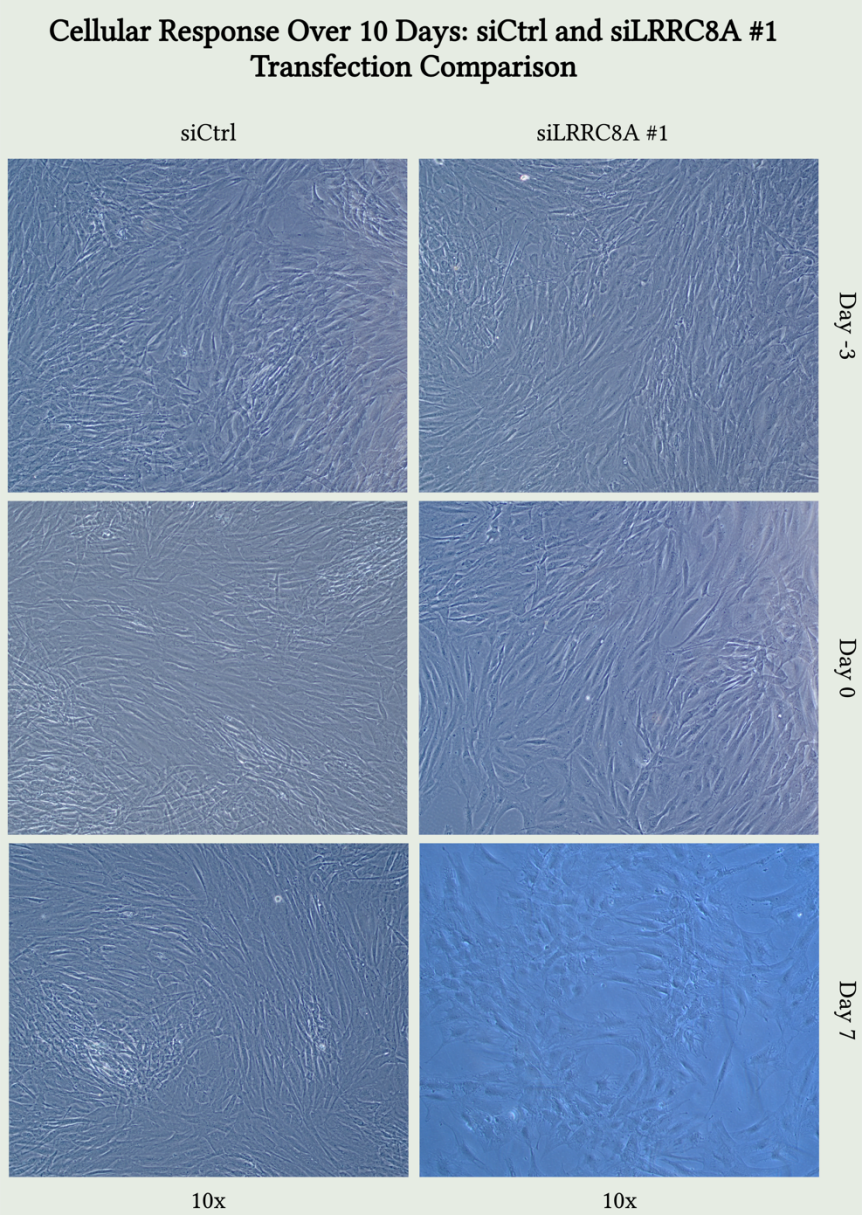

Figure 29

Figure 30 depicts fold change of LRRC8A where the fold change for siCtrl group remains consistent throughout, remaining very close to 1, indicating no significant variation over time. Conversely, siLRRC8A group decreased significantly from control at all time points; showing reduced expression levels compared to control, with day 7 showing the lowest fold change levels compared to the control group, indicating its success at reducing LRRC8A in SAT.

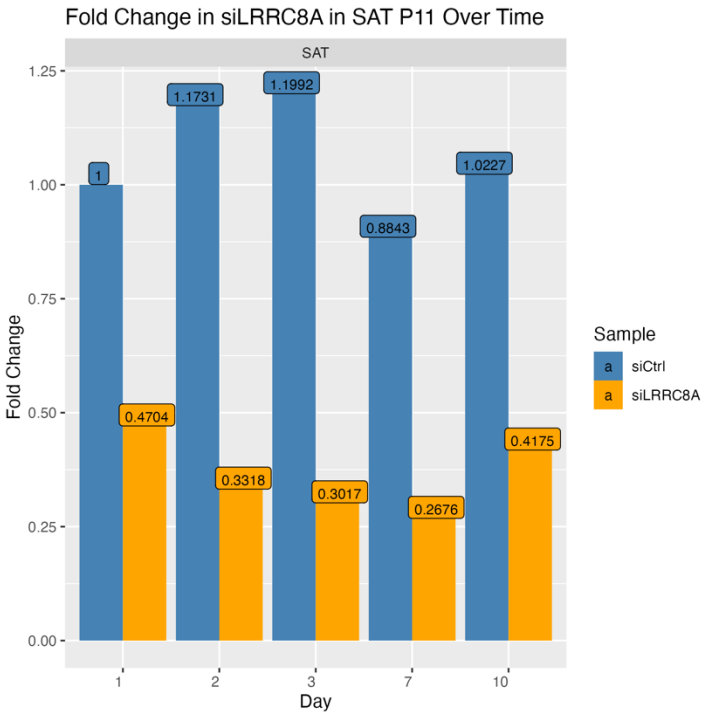

Figure 30 LRRC8A Expression Trends in SAT Over Time

A Time-Course Study to Assess of LRRC8A Knockdown Stability Over Time on VAT

This transfection experiment was designed to assess the duration of LRRC8A suppression in VAT cells with passage number 11, after transfection, to confirm its stability and the sustained knockdown for later experiments. In Figure 31 we can observe cells at time points from day 0 to day 10. On day 0 there is no apparent distinction between the control group and the siLRRC8A treated cells. By the day 3 one might expect to see some changes due to gene silencing. However, the micrographs do not reveal any differences between the two conditions. If LRRC8A silencing significantly affects cell morphology or proliferation, we would anticipate these differences to be evident by day 10. Nevertheless, the images do not show any alterations. Although all days and treatments the cell morphology remains consistent, with spindle shaped fibroblasts. There is no indication of cell death drastic changes, in appearance or major shifts in cell density that one would typically associate with the loss of a vital genes function. Additionally, it is crucial to validate the efficiency of LRRC8A knockdown

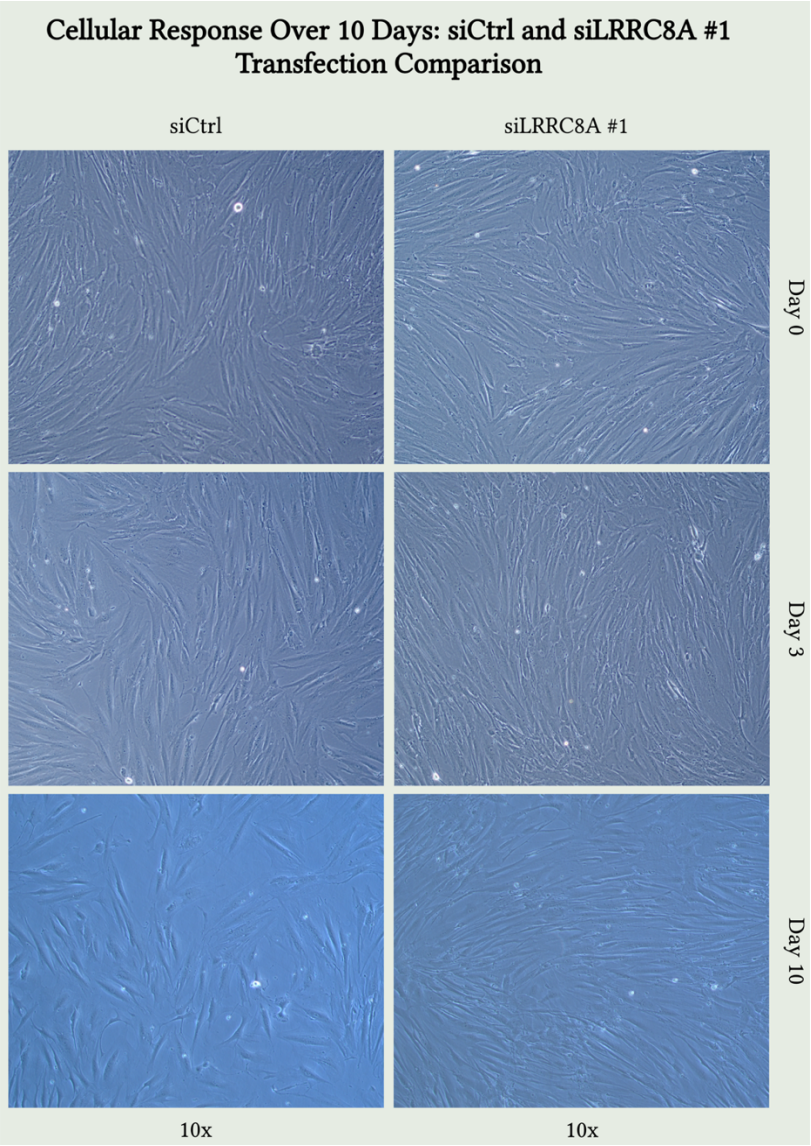

Figure 31

at the mRNA level in order to confirm the effectiveness of the siLRRC8A, which we have done later using qPCR.

Figure 32 shows the fold change in response to siLRRC8A treatment. At day 1 both groups were normalized to a change of 1 serving as a baseline for comparison. Starting from day 1 there is a decrease in change within the siLRRC8A treated group indicating that the treatment effectively reduces the expression of the LRRC8A. This suppression continues until day 3 with a recovery by day 7 suggesting that the cells might partially regain their state or adapt to the treatment. On the other hand, the control group shows fluctuations as expected since it is not affected by siRNA targeting LRRC8A. The consistent expression stability in the control groups further confirms that observed effects are specifically related to siRNA activity in the treatment group. It is worth noting that if LRRC8A is involved in stress response, the rebound at day 7 could indicate a mechanism at play. Such mechanism maybe adaptive response, which is commonly observed when genes are suppressed for a period (Li *et al.*, 2020).

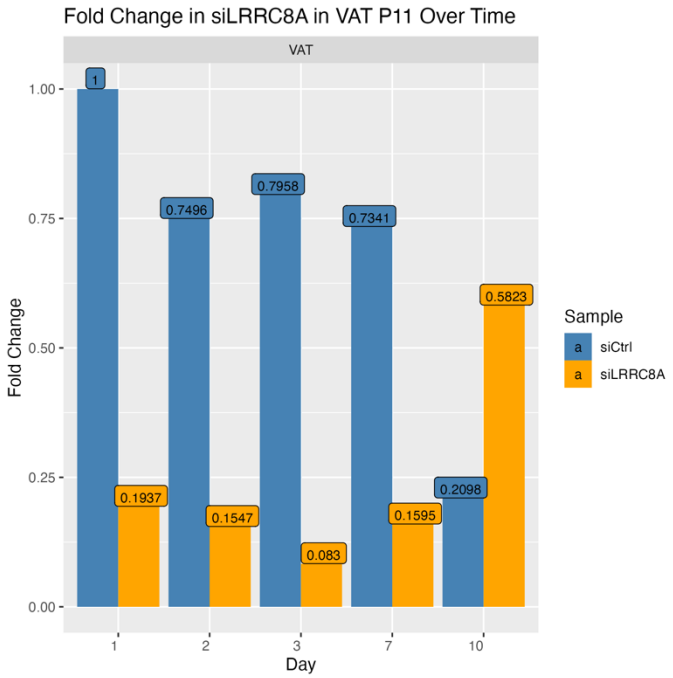

Figure 32 siRNA Impact on LRRC8A Expression in VAT

A Second Time-Course Study to Assess of LRRC8A Knockdown Stability Over Time on VAT

This transfection experiment was designed to assess the duration of LRRC8A suppression in VAT cells with passage number 10, after transfection, to confirm its stability and the sustained knockdown for later experiments. Transfection were started at day 0. At first glance, cells from both conditions appear similar in shape – an expected result post-transfection (Figure 33). From day 5 to 9, one would typically observe changes in cell morphology that would indicate responses to treatments, however both conditions here exhibited the elongated spindle-shaped characteristic of cells despite siRNA treatment; suggesting either that any responses might not be detectable with 10x magnification used or they have delayed or changes due to siRNA's influence. siRNA knockdown may affect specific cellular pathways or responses that LRRC8A plays a part in, which could explain why there were to notable morphological differences in the siLRRC8A #1 group compared with the control group. The absence of expected changes illustrated the fact that cell responses may differ depending on cell type of experimental conditions.

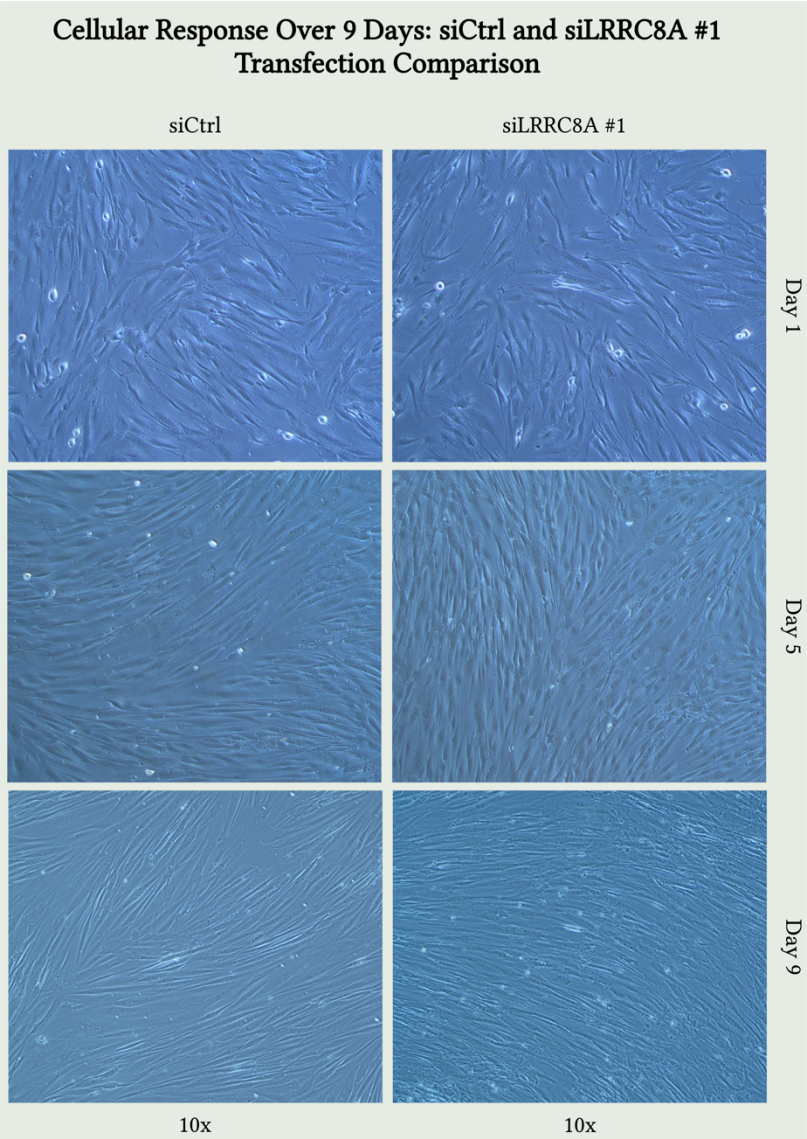

Figure 33

Figure 34 shows fold change in LRRC8A expression in VAT cells. Transfection started at day 0. On day 1 there was a decrease in fold change in the group indicating that the siRNA had an immediate effect on reducing gene expression. This trend continued throughout all time points with the siLRRC8A group showing fold changes compared to the control. Interestingly, on day 5 and 9 there were an increase in fold change for siLRRC8A surpassing that of the control. This could suggest either a rebound effect where cells compensate for knockdown or a shift in physiology as they differentiate (Rouf et al., 2023). The control groups fold change fluctuated slightly. However, its stable expression serves as a reference point to evaluate the effects of siLRRC8A on gene expression. The rebound effect along with the process of maturation highlights the relationship between gene regulation and cell development.

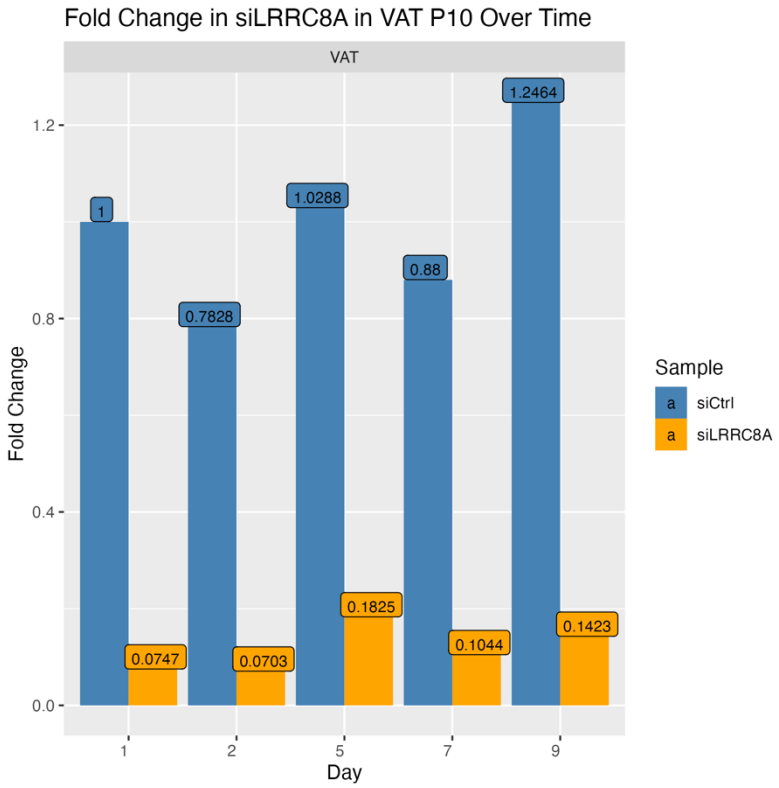

Figure 34 siRNA Effects on LRRC8A in VAT cells

The time-course experiments

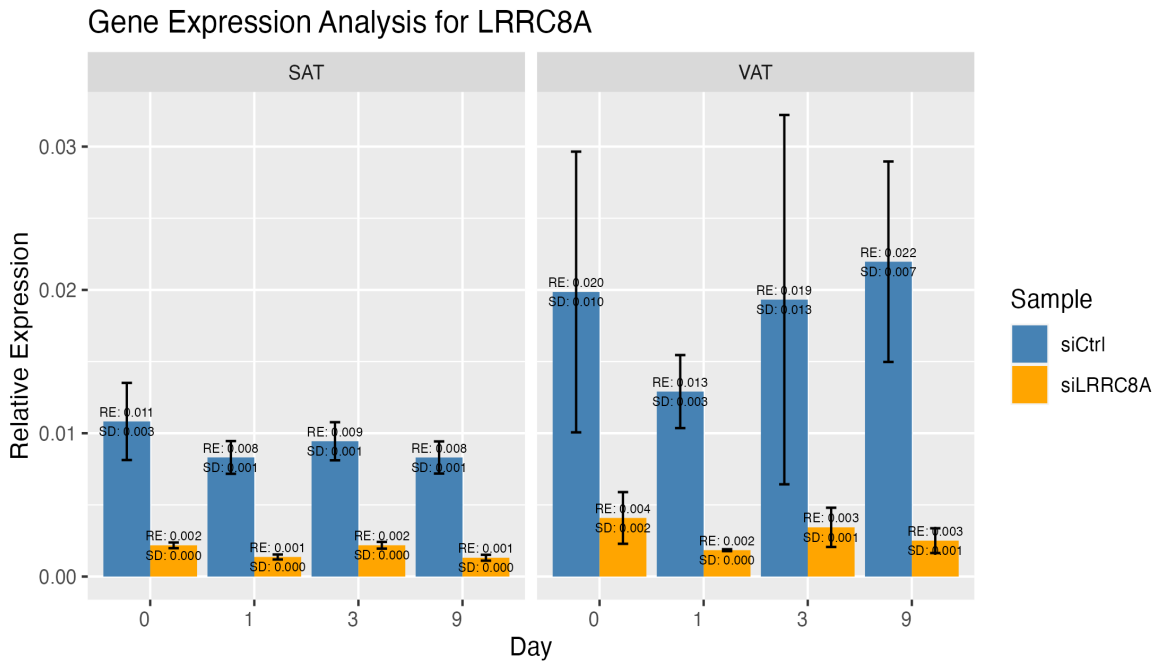

Figure 35

We performed a time-course experiments where we used triples of SAT cells (SAT P7, SAT P10, SAT P7) and another triplet of VAT cells (VAT P8, VAT P9 & VAT P9). The chart in Figure 35 displays a gene expression average of qPCR analysis for LRRC8A where two SAT & VAT were transfected on day 0 and differentiated on day 1. Focusing on the levels of expression in both SAT and VAT siCtrl maintains a stable LRRC8A expression. There are fluctuations within the range of experimental variation. However, in the treatment group siLRRC8A there is a reduction in LRRC8A expression on day 1 for both SAT and VAT cells. This indicates a knockdown. By day 3 the levels of expression in siLRRC8A group slightly remain below those of the control group, but slightly higher than siLRRC8A group on day 1. This suggests that there is a less pronounces effect of siLRRC8A. The error bars represent the range of variability among the replicates. The larger error bars seen in VAT on day 3 indicate a range of responses to the siRNA treatment. This could be due to differences in the adaptability or resilience of this type of adipose tissue during differentiation. The rise in VAT siLRRC8A group on day 3 and 9 could

suggest that there is a mechanism at the tissue level that compensates for the decreased expression of LRRC8A.

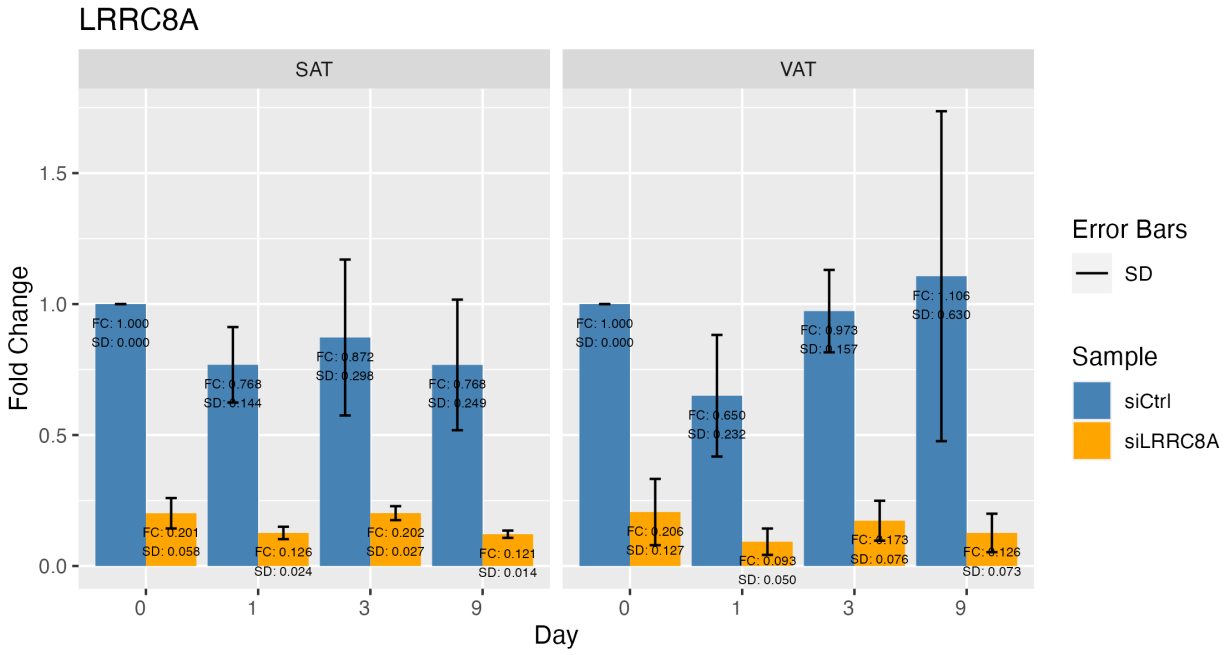

Figure 36

The chart in Figure 36 displays the fold change in LRRC8A expression in SAT and VAT cells. In SAT there is a decrease in expression siLRRC8A group across all days ranging from 0.2 to 0.12 compared to siCtrl. In VAT siCtrl group we observe a trend on day 1 and 3. On day 9 these is an unexpected increase in expression with a significant error bar indicating high variability among the samples. The error bars represent the deviation SD, providing information about the variability in the data. Larger bars indicate dispersion of values around the mean. In SAT the variability remains relatively stable suggesting that the response to siRNA treatments is more consistent in this tissue type. On the other hand, the large SD on day 9 in VAT suggests responses which may imply complex regulatory mechanisms. Considering similar studies, we can interpret that knockdown in SAT may suggest a simpler role of LRRC8A in these cells or a more consistent response to siRNA treatment. The differences in how VAT responds could offer insights into the mechanisms that regulate gene expression. These mechanisms can be influenced by factors like specific networks that control tissues. To summarize, the data introduced indicated that treating with siLRRC8A effectively reduces LRRC8A expression in both SAT and VAT. However, there is a variation in the tissue at a later time point.

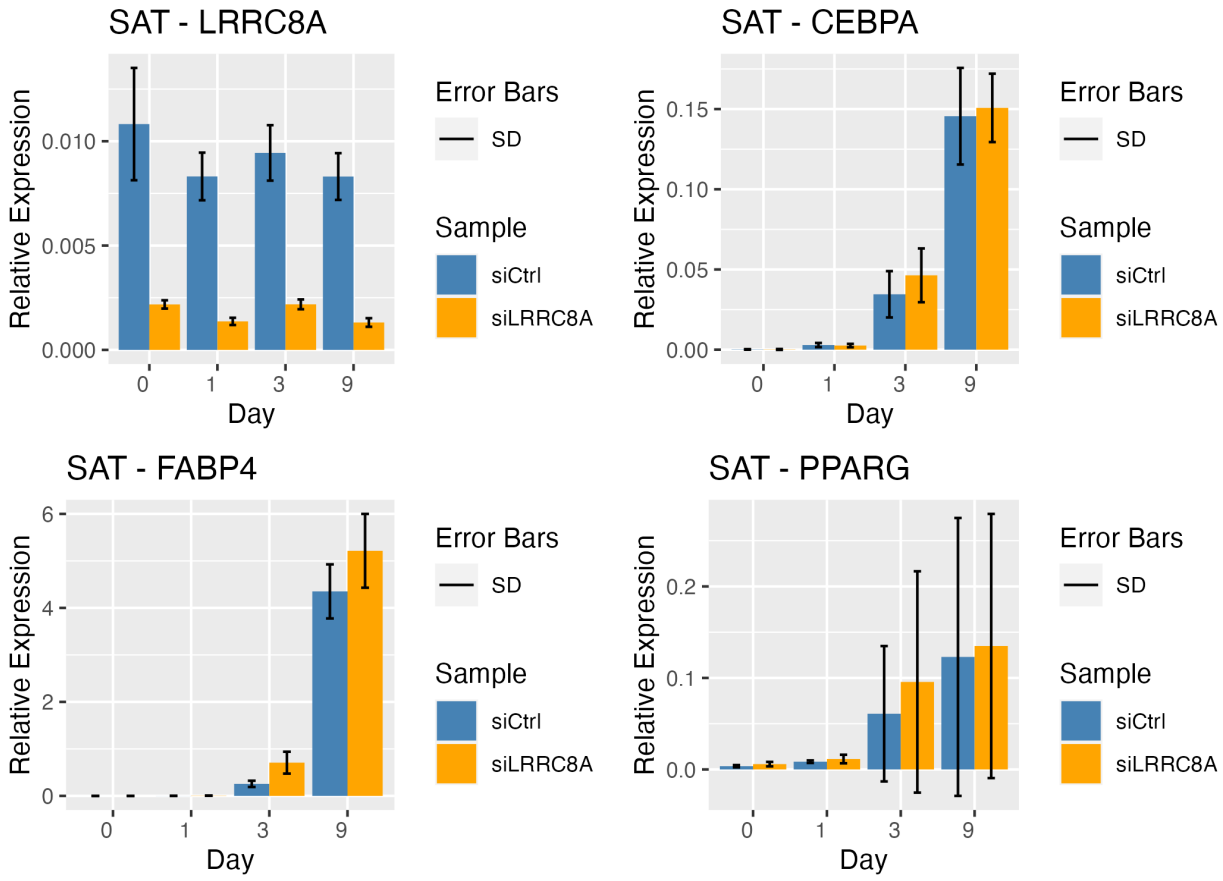

Figure 37

The bar chart in Figure 37 over provides information on the relative expression levels of the four genes: LRRC8A, CEBPA, FABP4 and PPARG. We used these genes in our experiment because they play a role in adipocyte function and differentiation making their expression patterns very informative. Starting with LRRC8A chart, it is the same chart that we presented earlier, now in comparison to the other genes. The expression of CEBPA appears to be normal in the siLRRC8A group on day 9. This suggests that there is no connection between LRRC8A activity and CEBPA expression or an effect of siRNA on this gene. It is the same case to the other genes; FABP4 and PPARG expression levels. The difference may lay in PPARG, where the expression levels vary the most. As it is showing a range of expression levels on da9 where the large error bars indicate high variability within the sample population. PPARG plays a role in regulating

adipogenesis and its varying expression might reflect differences in the response or differentiation state due to siRNA treatment (Hamza *et al.*, 2009).

In summary, the data shows a successful and sustained knockdown of LRRC8A and indicates complex and variable effects on other important genes involved in adipocyte differentiation.

The charts in Figure 38 display how genes LRR8CA, CEBPA, FABP4 and PPARG are expressed in VAT cells over a span of 9 days. On day 0 siRNA was used to transfect the cells

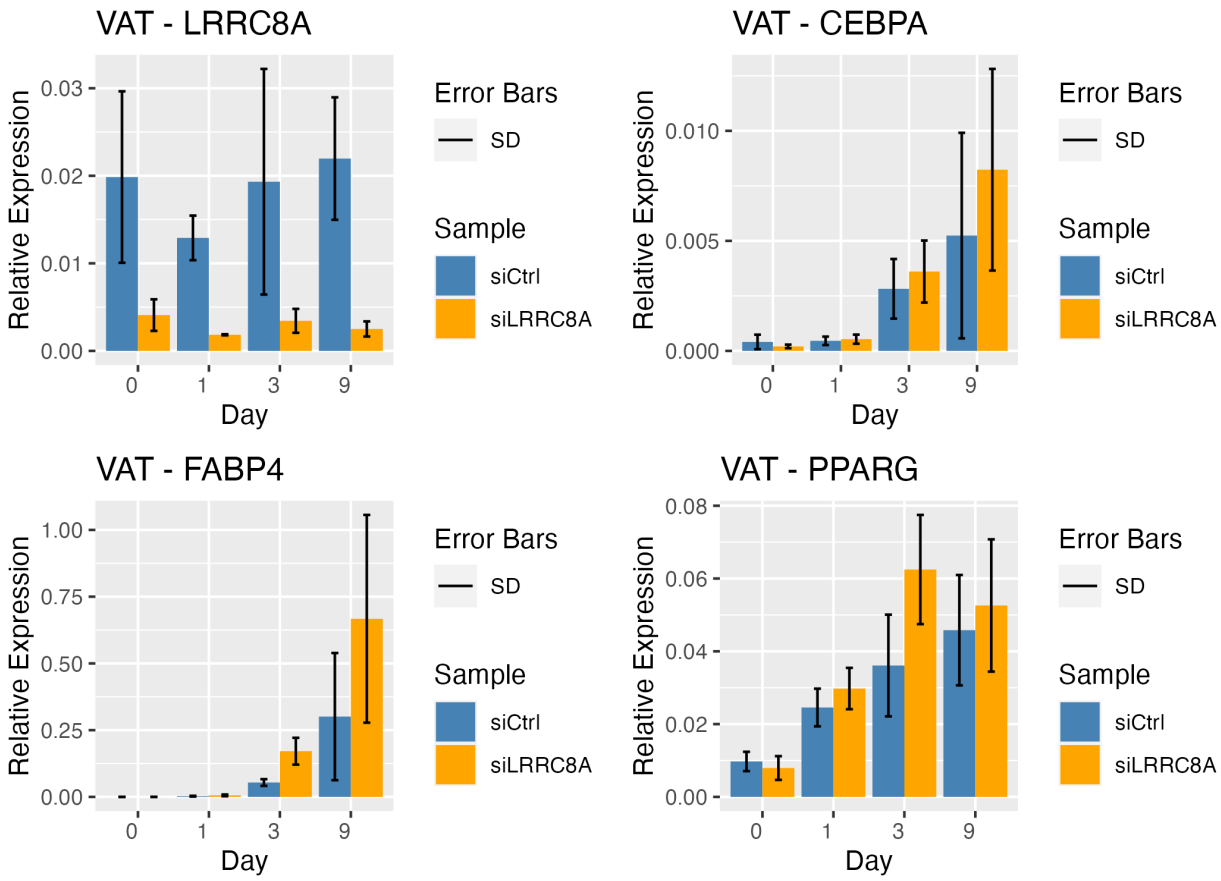

Figure 38

and differentiation began on day 1. LRRC8A charts were presented and commented earlier in this study. Over time we can observe an increase in CEBPA expression in the siLRRC8A group reaching its peak on day 9. While FABP4 expression initially decreases on day 1 then shows increase variability as time progress. The standard deviation bars widen on day 9. Through the period PPARG expression remains higher in the siLRRC8A group compared to the control

group. While on day 9 there is an increase in variability. These fluctuations could reflect how LRRC8A knockdown affects the process of cellular differentiation. There is an amount of variation in the data shown by the error bars on day 9 for CEBPA, FABP4 and PPARG.

In summary, it seems that the treatment with siLRRC8A reduces LRRC8A expression and also affects genes that play a role in adipocyte function and differentiation**.** The observed variability at later time points highlights how gene expression regulation during differentiation is complex and dynamic.

Statical analysis & methods

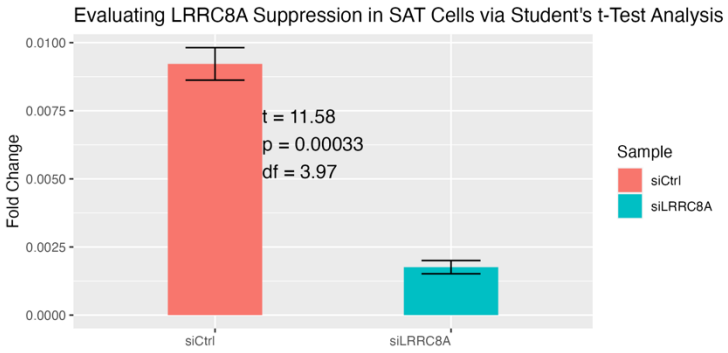

Figure 39

Figure 39 displays a bar graph that compares the change in LRRC8A gene expression between the two groups, siCtrl and siLLRC8A in SAT cells. The statistical information shown includes a t-value of 11.58, a p-value of 0.00033 and degrees of freedom (df) equal to 3.97. The t-value indicate difference between the means of the two groups compared to the variability observed within each group. The substantial t-value and low p-value strongly indicate that the difference in mean expression levels between these two groups is not due to change. Additionally, non-overlapping confidence interval shown by error bars further supports the conclusion that there is a difference in means between these groups. The combination of a p-value, t-value and non-overlapping confidence intervals provide compelling evidence that LRRC8A expression is significantly reduced in the siLRRC8A group compared to the siCtrl group.

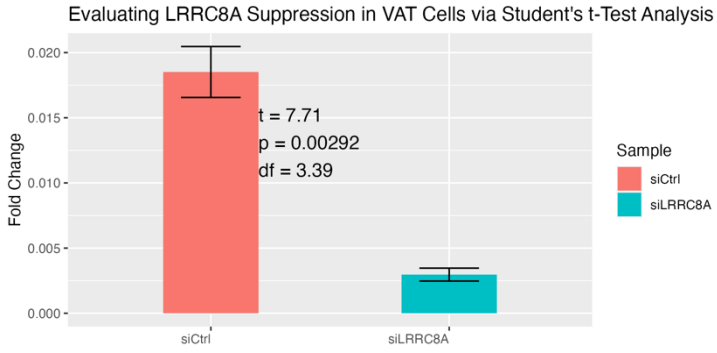

Figure 40

Figure 40 is a bar chart that shows the fold change in siCtrl vs siLRRC8A in VAT cells. It compares the two groups siCtrl and siLRRC8A. The figure shows a t-value of 7.71 and a p-value of 0.00292 with df of 3.39. With a t-value of 7.71 and a p-value less than 0.05 is strongly suggests that there is a statistical difference in gene expression between these two groups. The error bars shown on each bar represent the 95% confidence interval for the

change in each group. These findings demonstrate a decrease in LRRC8A expression within the siLLRC8A group confirming that the knockdown was successful. The considerable reduction in expression as indicated by both significance and effect size aligns with a silencing of the LRRC8A gene in VAT cells.

Discussion

Our research aimed to investigate the role of LRRC8A in the process of transforming preadipocytes into adipocytes, in both SAT and VAT. To study this, we utilized knockdown techniques, an established method to analyse how LRRC8A impacts adipocyte biology. Consistently our results from Western Blot and RT-qPCR analyses demonstrated a decrease in LRRC8A expression after siRNA treatment. This suggests that LRRC8A plays a role in adipogenesis. These findings align with studies that have emphasized the involvement of LRRC8A in regulating cell volume and promoting adipocyte differentiation (Jentsch et al., 2016; Strange et al., 2019). The distinct responses observed between SAT and VAT cells during our time-course experiments might offer insights into the role of LRRC8A within types of adipose tissue highlighting the complexity of adipose tissue biology. Our findings contribute to our understanding of obesity and metabolic disease. By uncovering the aspects of LRRC8A in the differentiation process of adipocytes, we shed light on targets for developing therapeutic interventions to address obesity related disorders. This is particularly relevant given the increasing rates of obesity and its associated health complications. To ensure the accuracy of our findings and minimize any errors we incorporated control measures, such as Actin, Lamin and GAPDH into Western blot assays. This approach validated that the observed changes in LRRC8A expression were not artifacts stemming from variations. Our selection of siRNA #1 over #2 was based of factors like effectiveness, simplicity and cost efficiency which are crucial when conducting research that could have clinical applications. The application of siRNA treatments effectively reduced the expression of LRRC8A while also revealing impacts on markers such as CEBPA, FABP4 and PPARG. these findings suggest that LRRC8A might interact with pathways involved in the differentiation of adipocytes. The variability observed in the response of VAT cells emphasized the nature of tissue biology. Underscores the significance of personalized approaches to combat obesity. Although our study has provided insights into the role plays by LRRC8A in adipogenesis it also highlights how complex adipocyte biology can be. This emphasizes the need for research to fully comprehend how LRRC8A interacts with pathways associated with adipogenesis and explore its potential as a target for metabolic

diseases. Moreover, it would be valuable to explore the long-term impacts of reducing LRRC8A and its influence on the functionality of adipocytes.

Our statistical tests, including Student's t-test and power analysis revealed differences in LRRC8A expression following treatment. This confirms the effectiveness of our approach to knockdown LRRC8A.

This investigation could offer insights for the development of strategies aimed at tackling obesity. However, it has also revealed the nature of adipocyte biology. Emphasized the need for further investigation. Future research could delve into how LRRC8A interacts with pathways involved in adipogenesis as well as its potential as a therapeutic target for metabolic diseases. Additionally, examining the long-term effects of reducing LRRC8A expression and its impact on adipocyte function could yield information for developing strategies to address obesity.

When conducting research involving tissue samples such as SAT and VAT, ethical considerations hold significant importance. In our study, we strictly adhered to principles by ensuring the confidentiality of the participants data before obtaining tissue samples. Personal information was detached from both samples and analysis data to ensure privacy protection.

Conclusion

Our study effectively demonstrated the role of LRRC8A in adipogenesis and its influence on crucial genes related to adipocyte differentiation. These findings not only advance our understanding of the mechanisms behind adipose tissue development but also open up possibilities for targeted interventions against obesity and metabolic diseases.

References

Arunachalam, K. and Sasidharan, S.P. (2021). "Protein Extraction and Western Blot Analysis," *Springer Protocols* [Preprint]. Available at: https://doi.org/10.1007/978-1-0716-1233-0_22.

Beta Actin and GAPDH: The importance of Western blot loading controls (no date). https://www.novusbio.com/antibody-news/antibodies/the-importance-of-beta-actin-and-gapdh-loading-controls.

Bio-Rad (no date) Western Blot Loading Controls | Bio-Rad. https://www.bio-rad-antibodies.com/western-blot-loading-controls-antibodies.html#:~:text=Lamin%20B1%20is%20commonly%20used,not%20contain%20a%20nuclear%20envelope.

Boccaletto, P., Stefaniak, F., Ray, A., Cappannini, A., Mukherjee, S., Purta, E., Kurkowska, M., Shirvanizadeh, N., Destefanis, E., Groza, P., Avşar, G., A, R., Pir, P., Dassi, E., Conticello, S. G., Aguilo, F., & Bujnicki, J. M. (2021). MODOMICS: a database of RNA modification pathways. 2021 update. *Nucleic Acids Research*, *50*(D1), D231–D235. https://doi.org/10.1093/nar/gkab1083

Britton, K. and Fox, C.S. (2011). 'Ectopic fat depots and cardiovascular disease,' Circulation, 124(24). https://doi.org/10.1161/circulationaha.111.077602.

Cawthorn, W. P., Scheller, E. L., & MacDougald, O. A. (2012). Adipose tissue stem cells meet preadipocyte commitment: going back to the future. *Journal of Lipid Research*, *53*(2), 227–246. https://doi.org/10.1194/jlr.r021089.

Chen, X. et al. (2022). 'LRRC8A critically regulates myofibroblast phenotypes and fibrotic remodeling following myocardial infarction,' Theranostics, 12(13), pp. 5824–5835. https://doi.org/10.7150/thno.75200.

Cohn, W. E. (1960). Pseudouridine, a Carbon-Carbon Linked Ribonucleoside in Ribonucleic Acids: Isolation, Structure, and Chemical Characteristics. *Journal of Biological Chemistry*, *235*(5), 1488–1498. https://doi.org/10.1016/s0021-9258(18)69432-3

Controls for RNAi experiments | Thermo Fisher Scientific - IE (no date). https://www.thermofisher.com/no/en/home/life-science/rnai/synthetic-rnai-analysis/controls-for-rnai-experiments.html.

Cristancho, A.G. and Lazar, M.A. (2011). "Forming functional fat: A growing understanding of adipocyte differentiation," *Nature Reviews Molecular Cell Biology*, 12(11), pp. 722–734. Available at: https://doi.org/10.1038/nrm3198.

Davidson, F. F., Matsha, T. E., Erasmus, R. T., Kengne, A. P., & Goedecke, J. H. (2019). The discriminatory power of visceral adipose tissue area vs anthropometric measures as a diagnostic marker for metabolic syndrome in South African women. *Diabetology & Metabolic Syndrome*. https://doi.org/10.1186/s13098-019-0483-1.

De Sá, P. M., Richard, A. J., Hang, H., & Stephens, J. M. (2017). Transcriptional Regulation of Adipogenesis. *Comprehensive Physiology*, 635–674. https://doi.org/10.1002/cphy.c160022.

Dominissini, D., Moshitch-Moshkovitz, S., Schwartz, S., Salmon-Divon, M., Ungar, L., Osenberg, S., Cesarkas, K., Jacob-Hirsch, J., Amariglio, N., Kupiec, M., Sorek, R., & Rechavi, G. (2012). Topology of the human and mouse m6A RNA methylomes revealed by m6A-seq. *Nature*, *485*(7397), 201–206. https://doi.org/10.1038/nature11112

Fox, C. S., Massaro, J. M., Hoffmann, U., Pou, K. M., Maurovich-Horvat, P., Liu, C., Vasan, R. S., Murabito, J. M., Meigs, J. B., Cupples, L. A., D'Agostino, R. B., & O'Donnell, C. J. (2007). Abdominal Visceral and Subcutaneous Adipose Tissue Compartments. Circulation, 116(1), 39–48. https://doi.org/10.1161/circulationaha.106.675355.

Garg, S. K., Maurer, H. M., Reed, K., & Selagamsetty, R. (2013). Diabetes and cancer: two diseases with obesity as a common risk factor. *Diabetes, Obesity and Metabolism*, *16*(2), 97–110. https://doi.org/10.1111/dom.12124.

Ghaben, A.L. and Scherer, P.E. (2019). 'Adipogenesis and metabolic health,' Nature Reviews Molecular Cell Biology, 20(4), pp. 242–258. https://doi.org/10.1038/s41580-018-0093-z.

Gregoire, F.M., Smas, C.M. and Sul, H.S. (1998). "Understanding Adipocyte Differentiation," *Physiological Reviews*, 78(3), pp. 783–809. Available at: https://doi.org/10.1152/physrev.1998.78.3.783.

Hamza, M.S. et al. (2009) 'De-Novo Identification of PPARγ/RXR Binding Sites and Direct Targets during Adipogenesis,' PLOS ONE, 4(3), p. e4907. https://doi.org/10.1371/journal.pone.0004907.

Ibrahim, M. (2010). Subcutaneous and visceral adipose tissue: structural and functional differences. Obesity Reviews, 11(1), 11–18. https://doi.org/10.1111/j.1467-789x.2009.00623.x.

Jentsch, T. J., & Pusch, M. (2018). CLC Chloride Channels and Transporters: Structure, Function, Physiology, and Disease. *Physiological Reviews*, *98*(3), 1493–1590. https://doi.org/10.1152/physrev.00047.2017.

Jentsch, T. J., Lutter, D., Planells-Cases, R., Ullrich, F., & Voss, F. K. (2016). VRAC: molecular identification as LRRC8 heteromers with differential functions. *Pflügers Archiv: European Journal of Physiology*, *468*(3), 385–393. https://doi.org/10.1007/s00424-015-1766-5.

Jia, G., Fu, Y., Wang, Y., Dai, Q., Zheng, G., Yang, Y., Yi, C., Lindahl, T. L., Pan, T., Yang, Y., & He, C. (2011). N6-Methyladenosine in nuclear RNA is a major substrate of the obesity-associated FTO. *Nature Chemical Biology*, *7*(12), 885–887. https://doi.org/10.1038/nchembio.687

Johnson, M. (2012). 'Loading controls for Western Blots,' Materials and Methods, 2. https://doi.org/10.13070/mm.en.2.114.

Kaisanlahti, A., & Glumoff, T. (2019). Browning of white fat: agents and implications for beige adipose tissue to type 2 diabetes. Journal of Physiology and Biochemistry, 75(1), 1–10. https://doi.org/10.1007/s13105-018-0658-5.

Kefauver, J. M., Saotome, K., Pallesen, J., Cottrell, C. A., Ward, A. B., & Patapoutian, A. (2018). Structure of human Volume Regulated Anion Channel composed of SWELL1 (LRRC8A). eLife. https://doi.org/10.2210/pdb6djb/pdb.

Kim, T.Y. and Eberwine, J. (2010). "Mammalian cell transfection: the present and the future," *Analytical and Bioanalytical Chemistry*, 397(8), pp. 3173–3178. Available at: https://doi.org/10.1007/s00216-010-3821-6.

Kurien, B.T. and Scofield, R.H. (2006). "Western blotting," *Methods*, 38(4), pp. 283–293. Available at: https://doi.org/10.1016/j.ymeth.2005.11.007.

Kusminski, C.M., Bickel, P.E. and Scherer, P.E. (2016). "Targeting adipose tissue in the treatment of obesity-associated diabetes," *Nature Reviews Drug Discovery*, 15(9), pp. 639–660. Available at: https://doi.org/10.1038/nrd.2016.75.

Lee, M., Wu, Y., & Fried, S. K. (2013). Adipose tissue heterogeneity: Implication of depot differences in adipose tissue for obesity complications. Molecular Aspects of Medicine, 34(1), 1–11. https://doi.org/10.1016/j.mam.2012.10.001.

Li, P. et al. (2020) 'LRRC8 family proteins within lysosomes regulate cellular osmoregulation and enhance cell survival to multiple physiological stresses,' Proceedings of the National Academy of Sciences of the United States of America, 117(46), pp. 29155–29165. https://doi.org/10.1073/pnas.2016539117.

Litovchick, L. (2020). "Immunoblotting," *CSH Protocols*, 2020(6), p. pdb.top098392. Available at: https://doi.org/10.1101/pdb.top098392.

MacPhee, D.J. (2010). "Methodological considerations for improving Western blot analysis," *Journal of Pharmacological and Toxicological Methods*, 61(2), pp. 171–177. Available at: https://doi.org/10.1016/j.vascn.2009.12.001.

Majka, S.M. *et al.* (2014). "Analysis and Isolation of Adipocytes by Flow Cytometry," *Methods in Enzymology*, pp. 281–296. Available at: https://doi.org/10.1016/b978-0-12-411619-1.00015-x.

Mardis, E. R. (2008). Next-Generation DNA Sequencing Methods. *Annual Review of Genomics and Human Genetics*, *9*(1), 387–402. https://doi.org/10.1146/annurev.genom.9.081307.164359.

Marin, R.D. *et al.* (2019). "RELi protocol: Optimization for protein extraction from white, brown and beige adipose tissues," *MethodsX*, 6, pp. 918–928. Available at: https://doi.org/10.1016/j.mex.2019.04.010.

Meyer, K. D., & Jaffrey, S. R. (2017). Rethinking m^{6}A Readers, Writers, and Erasers. *Annual Review of Cell and Developmental Biology*, *33*(1), 319–342. https://doi.org/10.1146/annurev-cellbio-100616-060758.

Midthjell, K., Lee, C., Langhammer, A., Krokstad, S., Holmen, T. L., Hveem, K., Colagiuri, S., & Holmen, J. (2013). Trends in overweight and obesity over 22 years in a large adult population: the HUNT Study, Norway. Clinical Obesity, 3(1–2), 12–20. https://doi.org/10.1111/cob.12009.

Müller, C. H., Zidek, L. M., Eichwald, S., Kortman, G., Koster, M. H., & Calkhoven, C. F. (2022). Enhanced C/EBPβ function promotes hyperplastic versus hypertrophic fat tissue growth and prevents steatosis in response to high-fat diet feeding. *eLife*, *11*. https://doi.org/10.7554/elife.62625.

O'Callaghan, J. P and Pierce. Rockford, IL. (2017). "Pierce BCA Protein Assay Protocol v1," *BCA Protein Assay Reagent (Instruction Manual)* [Preprint]. Available at: https://doi.org/10.17504/protocols.io.hrzb576.

Pant, R. et al. (2021) 'Epigenetic regulation of adipogenesis in development of metabolic syndrome,' Frontiers in Cell and Developmental Biology, 8. https://doi.org/10.3389/fcell.2020.619888.

Pedersen, S. F., Klausen, T. L., & Nilius, B. (2015). The identification of a volume-regulated anion channel: an amazing Odyssey. *Acta Physiologica*, *213*(4), 868–881. https://doi.org/10.1111/apha.12450.

Pillai-Kastoori, L., Schutz-Geschwender, A. and Harford, J.A. (2020) 'A systematic approach to quantitative Western blot analysis,' Analytical Biochemistry, 593, p. 113608. https://doi.org/10.1016/j.ab.2020.113608.

Qiu, Z., Dubin, A. E., Mathur, J., Tu, B., Reddy, K., Miraglia, L., Reinhardt, J., Orth, A. P., & Patapoutian, A. (2014). SWELL1, a Plasma Membrane Protein, Is an Essential Component of Volume-Regulated Anion Channel. *Cell*, *157*(2), 447–458. https://doi.org/10.1016/j.cell.2014.03.024.

Rocha, A. P., Guerra, B., Boucher, J., & Mori, M. A. (2021). A Method to Induce Brown/Beige Adipocyte Differentiation from Murine Preadipocytes. Bio-protocol, 11(24). https://doi.org/10.21769/bioprotoc.4265.

Rosen, E. D., & MacDougald, O. A. (2006). Adipocyte differentiation from the inside out. *Nature Reviews Molecular Cell Biology*, *7*(12), 885–896. https://doi.org/10.1038/nrm2066.

Rouf, M.A. et al. (2023). 'The recent advances and future perspectives of genetic compensation studies in the zebrafish model,' Genes and Diseases, 10(2), pp. 468–479. https://doi.org/10.1016/j.gendis.2021.12.003.

Rubino, S. et al. (2018). 'Downregulation of Leucine-Rich Repeat-Containing 8A limits proliferation and increases sensitivity of glioblastoma to temozolomide and carmustine,' Frontiers in Oncology, 8. https://doi.org/10.3389/fonc.2018.00142.

Saha, A., Kolonin, M. G., & DiGiovanni, J. (2023). Obesity and prostate cancer — microenvironmental roles of adipose tissue. *Nature Reviews Urology*, *20*(10), 579–596. https://doi.org/10.1038/s41585-023-00764-9.

Saltiel, A. R., & Olefsky, J. M. (2017). Inflammatory mechanisms linking obesity and metabolic disease. *Journal of Clinical Investigation*, *127*(1), 1–4. https://doi.org/10.1172/jci92035

Scheja, L., & Heeren, J. (2019). The endocrine function of adipose tissues in health and cardiometabolic disease. *Nature Reviews Endocrinology*, *15*(9), 507–524. https://doi.org/10.1038/s41574-019-0230-6

Sikkeland, J., Jin, Y. and Saatcioglu, F. (2014). "Methods to Assess Lipid Accumulation in Cancer Cells," *Methods in Enzymology*, pp. 407–423. Available at: https://doi.org/10.1016/b978-0-12-416618-9.00021-2.

siRNA Transfection (2023). Available at: https://cell-transfection.com/sirna-transfection/.

Stauber, T. (2015). The volume-regulated anion channel is formed by LRRC8 heteromers – molecular identification and roles in membrane transport and physiology. *Biological Chemistry*, *396*(9–10), 975–990. https://doi.org/10.1515/hsz-2015-0127.

Strange, K., Yamada, T., & Denton, J. S. (2019). A 30-year journey from volume-regulated anion currents to molecular structure of the LRRC8 channel. *The Journal of General Physiology*, *151*(2), 100–117. https://doi.org/10.1085/jgp.201812138

Swinburn, B., Sacks, G., Hall, K. D., McPherson, K., Finegood, D. T., Moodie, M., & Gortmaker, S. L. (2011). The global obesity pandemic: shaped by global drivers and local environments. The Lancet, 378(9793), 804–814. https://doi.org/10.1016/s0140-6736(11)60813-1.

Tanudji, M. et al. (2010). 'Competition Between siRNA Duplexes: Impact of RNA-Induced Silencing Complex Loading Efficiency and Comparison Between Conventional-21 bp and Dicer-Substrate siRNAs,' Oligonucleotides, 20(1), pp. 27–32. https://doi.org/10.1089/oli.2009.0195.

Taylor, S.V. *et al.* (2013). "A Defined Methodology for Reliable Quantification of Western Blot Data," *Molecular Biotechnology*, 55(3), pp. 217–226. Available at: https://doi.org/10.1007/s12033-013-9672-6.

Tchernof, A., & Després, J. (2013). Pathophysiology of Human Visceral Obesity: An Update. Physiological Reviews, 93(1), 359–404. https://doi.org/10.1152/physrev.00033.2011.

Thermofisher - Invitrogen (no date) *Transfecting stealth rnai or Sirna into human mesenchymal stem cells ...*, *https://www.thermofisher.com/*. Thermofisher - Invitrogen. Available at: https://origin-distributor.qa.cloudqa.thermofisher.com/content/dam/LifeTech/migration/en/filelibrary/pdf.par.99253.file.dat/protocols.par.65454.file.dat/human-mesenchymal-stem%20cells-rnaimax-25-0909w.pdf (Accessed: February 11, 2023).

Trayhurn, P. (2005). Adipose Tissue in Obesity—An Inflammatory Issue. Endocrinology, 146(3), 1003–1005. https://doi.org/10.1210/en.2004-1597.

Trayhurn, P. (2013). Hypoxia and Adipose Tissue Function and Dysfunction in Obesity. *Physiological Reviews*, *93*(1), 1–21. https://doi.org/10.1152/physrev.00017.2012

Villarroya, F., Cereijo, R., Villarroya, J., & Giralt, M. (2017). Brown adipose tissue as a secretory organ. *Nature Reviews Endocrinology*, *13*(1), 26–35. https://doi.org/10.1038/nrendo.2016.136

Voss, F. K., Ullrich, F., Münch, J., Lazarow, K., Lutter, D., Mah, N., Andrade-Navarro, M. A., Von Kries, J. P., Stauber, T., & Jentsch, T. J. (2014). Identification of LRRC8 Heteromers as an Essential Component of the Volume-Regulated Anion Channel VRAC. *Science*, *344*(6184), 634–638. https://doi.org/10.1126/science.1252826.

Wajchenberg, B. L. (2000). Subcutaneous and Visceral Adipose Tissue: Their Relation to the Metabolic Syndrome. Endocrine Reviews, 21(6), 697–738. https://doi.org/10.1210/edrv.21.6.0415.

Wang, S. et al. (2022) 'Dynamic regulation and functions of mRNA m6A modification,' Cancer Cell International, 22(1). https://doi.org/10.1186/s12935-022-02452-x.

Western blotting electrophoresis techniques (2023). https://www.bio-rad.com/en-no/applications-technologies/western-blotting-electrophoresis-techniques?ID=PQEENTWDLBV5.

Western blotting guide: Part 2, Protein separation by SDS-PAGE (2023). https://www.jacksonimmuno.com/secondary-antibody-resource/technical-tips/western-blotting-guide-part-2/#:~:text=Gradient%20gels%20are%20used%20to,on%20the%20protein%20separation%20required.

World Health Organization: WHO. (2021). Obesity and overweight. www.who.int. https://www.who.int/news-room/fact-sheets/detail/obesity-and-overweight.

Yang, C. et al. (2020). 'The role of m6A modification in physiology and disease,' Cell Death and Disease, 11(11). https://doi.org/10.1038/s41419-020-03143-z.

Yang, Ying et al. (2018). 'Dynamic transcriptomic m6A decoration: writers, erasers, readers and functions in RNA metabolism,' Cell Research, 28(6), pp. 616–624. https://doi.org/10.1038/s41422-018-0040-8.

Zhang, L. et al. (2015) 'PPIA is a novel adipogenic factor implicated in obesity,' Obesity, 23(10), pp. 2093–2100. https://doi.org/10.1002/oby.21208.

Zhao, B. S., Roundtree, I. A., & He, C. (2017). Post-transcriptional gene regulation by mRNA modifications. *Nature Reviews Molecular Cell Biology*, *18*(1), 31–42. https://doi.org/10.1038/nrm.2016.132

Zhu, B. et al. (2021). 'Adipose tissue inflammation and systemic insulin resistance in mice with diet-induced obesity is possibly associated with disruption of PFKFB3 in hematopoietic cells,' Laboratory Investigation, 101(3), pp. 328–340. https://doi.org/10.1038/s41374-020-00523-z.

Appendix

List of Tables

Reagents & Equipment	Product number	Supplier	Amount
Subcutaneous human preadipocytes (SAT)	Zen-Bio	SP-F-3	LM050709B
Omental visceral human preadipocytes (VAT)	Zen-Bio	OP-F-3	OMM020216C
DMEM-F12 Glutamax	10565018	Gibco/ThermoFisher	500 ml
IBMX	I5879	SIGMA	0.5 mM
Dexamethasone	D4902	SIGMA	1 µl
Indomethacin	I7378-56	SIGMA	0.2mM
Insulin	I9278	SIGMA	
RIPA buffer	9806	Cell Signaling Technology	
Pierce Protease Inhibitor Tablets, EDTA-free	A32965	ThermoFisher Scientific	50 mL buffer per tablet
Pierce Protease Inhibitor Mini Tablets, EDTA-free	A32955	ThermoFisher Scientific	10 mL buffer per tablet
Pierce Protease Inhibitor XL Capsules, EDTA-free	A37989	ThermoFisher Scientific	500 mL buffer per tablet
Loading pipette			
Gel			
Electrophoresis chamber			
The molecular weight marker (MWM)			10 µl
Antibody: GAPDH; a loading control			1:10000 diluted in TBS

Antibody: anti-rabbit			1:2500 diluted in 5% dry milk in TBS-tween
Antibody: anti-Lamin B1 ab	ab16048	Abcam	1:1000 in TBS-tween
Antibody: Actin	ab1801	Abcam	1:1000 in TBS-tween
Antibody: LRRC8A	ab254389	Abcam	1:1000 in TBS-tween
Antibody: LRRC8A	24979	Cell Signalling	1:1000 in TBS-tween
TBS-tween			1:1000
Dry milk			5 %
Lipofectamine™ RNAiMAX Transfection Reagent, 0,3 ml	13778030	ThermoFisher Scientific	
Opti-MEM™ I Reduced Serum Medium, 100 ml	31985062	ThermoFisher Scientific	
Silencer Select siRNA for METTL3, 5 nmol #1	s32141	ThermoFisher Scientific	
Silencer Select siRNA for METTL3, 5 nmol	s32142	ThermoFisher Scientific	
Silencer Select Control siRNA no 1, 20 nmol	4390844	ThermoFisher Scientific	
FBS	Gibco/Thermo Fisher	10500-056	-20 °C
Pen. Strept			-20 °C
bFGF	Gibco/Thermo Fisher	PHG0264	-20 °C
TrypLE express		Gibco/Thermo Fisher	
PBS		Media kitchen	4 °C
Crushed ice			

RNeasy Mini Kit		Qiagen	
QIAzol, Chloroform			
70 % Ethanol			
RNase free water			
RNase removal spray			
Qiashredder			

Table 3 Typical volumes used for cell culture

Flask/well size	DMEM/F12 (ml)	PBS (ml)	TrypLE(ml)
6 well (9,6 cm^2)	2,5	1	0,2
25 cm^2	5	2	0,5
75 cm^2	15	10	1
175 cm^2	30	20	2.5

cDNA synthesis mastermix		
	1X	**12X**
10X Rt buffer	2	**24**
25X dNTP	0.8	**9.6**
10X RT random primers	2	**24**
Reverse transcriptase	1	**12**
Nuclease free water	4.2	**50.4**
Total	10	**120**

Name	*LRRC8A*	*Actin*	*LRRC8A/Actin_Ratio*	*LRRC8A_Actin_siCtrl*	*Lamin*	*LRRC8A/Lamin_Ratio*	*LRRC8A_Lamin_siCtrl*
siCtrl	*553552.3*	*438359.0*	*1.26278300*	*1.00000000*	*505423,1*	*1.0952256*	*1.0000000*
siLRRC8A #1	*166791.1*	*482298.0*	*0,3458259*	*0.27400000*	*739423,39*	*0.2255692*	*0.2060000*
siLRRC8A #2	*256612.2*	*611072.4*	*0,4199374*	*0.33300000*	*773100,91*	*0.3319258*	*0.3030000*
siLRRC8A #1 +	*154725.9*	*463552.8*	*0,3337828*	*0.26400000*	*512908,93*	*0.3016636*	*0.2750000*
No transfect	*705066.3*	*464697.6*	*1.51725800*	*1.20200000*	*557409,47*	*1.2648983*	*1.1550000*

Table shows Analyse, LRRC8A Expression normalized against Actin and Lamin expression for Optimization of conditions for siRNA knockdown using Western Blot experiment.

Table 4 Protein concentration and sample preparation data for experiment LRRC8A Protein Detection Through Western Blot

Sample	Protein concentration (µg/µl)	Per well (µg)	Sample (µl)	Sample buffer (µl)	Buffer 2 (µl)	Loading volum (µl)	Total volume (µl)
#1_SAT Protein lysis (1 mill cells)	1.0	20	88.4	42.5	39.1	40.0	170
#2_SAT Protein lysis (1 mill cells)	0.8	20	106.8	42.5	20.7	40.0	170
#3_SAT Protein lysis (1 mill cells)	0.8	20	109.7	42.5	17.8	40.0	170
#4_SAT Protein lysis (2 mill cells)	1.3	20	112.3	37.5	0.2	20.0	150
#5_SAT Protein lysis (2 mill cells)	1.4	20	106.7	37.5	5.8	20.0	150
#6, SAT Protein lysis (2 mill cells)	1.4	20	108.4	37.5	4.1	20.0	150

Table 5 Concentration Values for Calibration and Protein lysis Samples for Experiment LRRC8A Protein Detection Through Western Blot

Sample	1	2	3	4	5	6
A				#1_SAT Protein lysis 1/3	#1_SAT Protein lysis 2/3	#1_SAT Protein lysis 3/3
B	Calibrator_0002 1/3	Calibrator_0002 2/3	Calibrator_0002 3/3	#2_SAT Protein lysis 1/3	#2_ SAT Protein lysis 2/3	#2_SAT Protein lysis 3/3
C	Calibrator_0003 1/3	Calibrator_0003 2/3	Calibrator_0003 3/3	#3_SAT Protein lysis 1/3	#3_SAT Protein lysis 2/3	#3_SAT Protein lysis 3/3
D	Calibrator_0004 1/3	Calibrator_0004 2/3	Calibrator_0004 3/3	#4_SAT Protein lysis 1/3	#4_SAT Protein lysis 2/3	#4_SAT Protein lysis 3/3
E	Calibrator_0005 1/3	Calibrator_0005 2/3	Calibrator_0005 3/3	#5_SAT Protein lysis 1/3	#5_SAT Protein lysis 2/3	#5_SAT Protein lysis 3/3
F	Calibrator_0006 1/3	Calibrator_0006 2/3	Calibrator_0006 3/3	#6_SAT Protein lysis 1/3	#6_ SAT Protein lysis 2/3	#6_SAT Protein lysis 3/3
G						
H						

Value	1	2	3	4	5	6
A				920.2	933.7	1031.0
B	4.4	8.0	4.4	769.1	808.4	810.0
C	10.3	9.3	10.6	744.3	774.5	805.8
D	14.8	13.9	14.3	1281.3	1351.5	1374.6
E	20.9	20.4	19.7	1334.2	1411.0	1472.8
F	41.5	39.7	38.8	1324.2	1405.6	1421.2
G						
H						
Plate 1: 1	Blank Type: Average	Wavelength: 560	Fit to Assay: Calibrator	Fit Type: QuadraticPolynomial	Formula: Quadratic Polynomial: y = cx2 + bx + a	

Table 6. Gel Loading Pattern for Protein Analysis in Experiment WB232

Gel A

Extra well	Well #1	Well #2	Well #3	Well #4	Well #5	Well #6	Well #7	Well #8	Well #9	Well #10	Well #11	Well #12	Extra well
MWM	Sample #4 (10 µl)	Sample #5 (10 µl)	Sample #6 (10 µl)	MWM	Sample #4 (20 µl)	Sample #5 (20 µl)	Sample #6 (20 µl)	MWM	Sample #4 (30 µl)	Sample #5 (30 µl)	Sample #6 (30 µl)	MWM	

Gel B

Extra well	Well #1	Well #2	Well #3	Well #4	Well #5	Well #6	Well #7	Well #8	Well #9	Well #10	Well #11	Well #12	Extra well
MWM	Sample #4 (10 µl)	Sample #5 (10 µl)	Sample #6 (10 µl)	MWM	Sample #4 (20 µl)	Sample #5 (20 µl)	Sample #6 (20 µl)	MWM	Sample #4 (30 µl)	Sample #5 (30 µl)	Sample #6 (30 µl)	MWM	

The WB gel is a gradient gel (4-15% gels), in which they are capable of differentiating proteins over a broader kDA range. The gel has two additional specialized wells on the outer edges designed for the marker (MWM) with a reduced loading capacity. The gels contain 12 wells with a capacity of max 45 µl/well.

Table 7 Concentration Values for Calibration and Protein lysis Samples for Experiment WB233

Sample	1	2	3	4	5	6
A	Calibrator_0001 1/3	Calibrator_0001 2/3	Calibrator_0001 3/3	siCtrl 1/3	siCtrl 2/3	siCtrl 3/3
B	Calibrator_0002 1/3	Calibrator_0002 2/3	Calibrator_0002 3/3	siLRRC8A #1	siLRRC8A #1	siLRRC8A #1
C	Calibrator_0003 1/3	Calibrator_0003 2/3	Calibrator_0003 3/3	siLRRC8A #2	siLRRC8A #3	siLRRC8A #4
D	Calibrator_0004 1/3	Calibrator_0004 2/3	Calibrator_0004 3/3	siLRRC8A # (1 + 2)	siLRRC8A # (1 + 2)	siLRRC8A # (1 + 2)
E	Calibrator_0005 1/3	Calibrator_0005 2/3	Calibrator_0005 3/3	No Transfection	No Transfection	No Transfection
F	Calibrator_0006 1/3		Calibrator_0006 3/3			
G	Blank Assay 1	Blank Assay 2	Blank Assay 3			
H						

Value	1	2	3	4	5	6
A	0.6	0.6	0.4	665.3	655.4	652.9
B	4.6	4.3	4.4	650.0	652.1	661.0
C	9.5	9.4	9.5	735.8	718.5	720.2
D	15.1	14.8	14.8	569.6	564.6	549.8
E	21.4	20.2	20.7	641.8	635.5	638.4
F	29.9	NaN	36.8			
G	0.5	0.5	0.5			
H						
Plate 1: 1	Blank Type: Average	Wavelength: 560	Fit to Assay: Calibrator	Fit Type: QuadraticPolynomial	Formula: Quadratic Polynomial: y = cx2 + bx + a	

Table 8 Concentration Values for Calibration and Protein lysis Samples for Experiment WB234

Sample	1	2	3	4	5	6
A	Calibrator_0001 1/3	Calibrator_0001 2/3	Calibrator_0001 3/3	#1_VAT Protein lysis 1/3	#1_VAT Protein lysis 2/3	#1_VAT Protein lysis 3/3
B	Calibrator_0002 1/3	Calibrator_0002 2/3	Calibrator_0002 3/3	#2_VAT Protein lysis 1/3	#2_VAT Protein lysis 2/3	#2_VAT Protein lysis 3/3
C	Calibrator_0003 1/3	Calibrator_0003 2/3	Calibrator_0003 3/3	#3_VAT Protein lysis 1/3	#3_VAT Protein lysis 2/3	#3_VAT Protein lysis 3/3
D	Calibrator_0004 1/3	Calibrator_0004 2/3	Calibrator_0004 3/3	#4_VAT Protein lysis 1/3	#4_VAT Protein lysis 2/3	#4_VAT Protein lysis 3/3
E	Calibrator_0005 1/3	Calibrator_0005 2/3	Calibrator_0005 3/3	#6_VAT Protein lysis 1/3	#5_VAT Protein lysis 2/3	#5_VAT Protein lysis 3/3
F	Calibrator_0006 1/3	Calibrator_0006 2/3	Calibrator_0006 3/3	#5_VAT Protein lysis 1/3	#6_VAT Protein lysis 2/3	#6_VAT Protein lysis 3/3
G	Blank Assay 1	Blank Assay 2	Blank Assay 3			
H						

Value	1	2	3	4	5	6
A	0.1	0.1	0.1	498.4	428.9	474.6
B	4.7	4.6	4.7	612.8	502.9	554.4
C	9.9	10.0	9.9	608.2	525.0	536.3
D	14.8	14.2	14.9	667.7	697.7	571.5
E	20.3	20.2	20.4	761.2	720.1	717.0
F	40.9	39.1	39.6	10.2	18.1	18.9
G	0.0	0.0	0.0			
H						
Plate 1: 1	Blank Type: Average	Wavelength: 560	Fit to Assay: Calibrator	Fit Type: QuadraticPolynomial	Formula: Quadratic Polynomial: y = cx2 + bx + a	

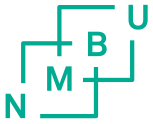

Norges miljø- og biovitenskapelige universitet
Noregs miljø- og biovitskapelege universitet
Norwegian University of Life Sciences

Postboks 5003
NO-1432 Ås
Norway